HHS Public Access

Author manuscript

J Labelled Comp Radiopharm. Author manuscript; available in PMC 2019 July 01.

Published in final edited form as:

J Labelled Comp Radiopharm. 2018 July ; 61(9): 693–714. doi:10.1002/jlcr.3622.

Aligning physics and physiology: Engineering antibodies for radionuclide delivery

Wen-Ting K. Tsai and **Anna M. Wu**

Crump Institute for Molecular Imaging, Department of Molecular and Medical Pharmacology, David Geffen School of Medicine at UCLA, Los Angeles, CA, USA

Abstract

The exquisite specificity of antibodies and antibody fragments renders them excellent agents for targeted delivery of radionuclides. Radiolabeled antibodies and fragments have been successfully used for molecular imaging and radioimmunotherapy (RIT) of cell-surface targets in oncology and immunology. Protein engineering has been employed for antibody humanization essential for clinical applications, as well as optimization of important characteristics including pharmacokinetics, biodistribution, and clearance. Although intact antibodies have high potential as imaging and therapeutic agents, challenges include long circulation time in blood, which leads to later imaging time points post-injection and higher blood absorbed dose that may be disadvantageous for RIT. Utilizing engineered fragments may address these challenges, as size reduction and removal of Fc function decreases serum half-life. Radiolabeled fragments and pretargeting strategies can result in high contrast images within hours to days, and a reduction of RIT toxicity in normal tissues. Additionally, fragments can be engineered to direct hepatic or renal clearance, which may be chosen based on the application and disease setting. This review discusses aligning the physical properties of radionuclides (positron, gamma, beta, alpha, and Auger-emitters) with antibodies and fragments, and highlights recent advances of engineered antibodies and fragments in preclinical and clinical development for imaging and therapy.

INTRODUCTION

Antibodies enable highly specific delivery of radionuclides for imaging and therapy and can target a wide range of cell-surface biomarkers, including antigens expressed on cancer cells and immune cells. The high specificity of antibodies is advantageous for noninvasive whole body molecular imaging, such as single-photon emission computed tomography (SPECT) and positron emission tomography (PET). Antibody-based PET imaging (immunoPET) in the clinic has improved resolution, sensitivity, and quantitation compared to SPECT, and it has been employed in oncology to guide therapy selection, estimate dosimetry for radioimmunotherapy, and track response to therapy[1,2]. In addition to imaging oncological targets, immunoPET has been employed to detect and track immune cells, and it can also be

Corresponding author: Anna M. Wu, Crump Institute for Molecular Imaging, University of California, Los Angeles, 570 Westwood Plaza, PO Box 951770, Los Angeles, CA 90095, USA, Tel: 1 (310) 794-5088, Fax: 1 (310) 206-8975, awu@mednet.ucla.edu.

DISCLOSURE OF POTENTIAL CONFLICTS OF INTEREST:

A. Wu has ownership interest in, and is a consultant/advisory board member for ImaginAb, Inc.

used to monitor inflammation and immune responses[2]. The precise specificity of antibodies also offers the potential for highly targeted delivery of radionuclides for radioimmunotherapy (RIT). Antibodies targeting a spectrum of cell surface markers have shown efficacy of RIT in hematopoietic cancers and to a lesser extent, solid tumors[3]. Importantly, the same antibody can be used for diagnostic imaging as well as RIT, a classic example of "theranostics", where imaging can provide key information on antigen expression, delivery of the therapeutic agent, dosimetry, and response to therapy.

Over the years, properties of classic intact murine monoclonal antibodies have been modified to optimize their clinical utility, and the current progress of engineered antibodies has been discussed in several reviews[4,5]. The vast majority of current therapeutic antibodies are thus based on humanized or human antibodies to reduce immunogenicity and enhance effector functions in patients. Furthermore, monoclonal antibodies have proven to be versatile carriers of a variety of cargoes for diagnostic as well as therapeutic purposes. Here, we review the additional contributions of protein engineering to the optimization of antibodies for targeted radionuclide delivery.

The intact IgG antibody (~150 kDa) is composed of antigen-binding (Fab) domains and a constant region (Fc) that interacts with cell-surface receptors, such as Fc_{γ} receptors ($Fc_{\gamma}R$) on immune effector cells (Figure 1a). The Fc also interacts with the neonatal Fc receptor (FcRn), which is involved in antibody recycling and maintenance in the circulation. Challenges with the use of radiolabeled intact antibodies for imaging and therapy include long circulating half-life (days to weeks) due to the size and FcRn interaction, as well as potential biological effects from interactions with Fc receptors (e.g., $Fc_{\gamma}R$) on immune effector cells. In imaging applications, this results in high background from circulating activity that can require delayed imaging for optimal contrast[6]. While obtaining high tumor-to-background contrast at specific time points is important for imaging, high therapeutic index is more relevant for therapy. Advantages of using a radiolabeled intact antibody for RIT include the ability to deliver a significant dose to the target tumors, but this strategy may also lead to high radiation exposure to normal tissues. Thus, development of antibodies for diagnostic imaging or RIT requires optimization of several characteristics, including pharmacokinetics, biodistribution, and clearance. Additional considerations include target characteristics (tumor expression, normal tissue expression, internalization, etc.), disease and setting (hematopoietic vs solid tumor, radiosensitivity, lesion size, etc.). Protein engineering can be applied to optimize affinity, improve pharmacokinetics, enable uniform conjugation/radiolabeling, and guide excretion towards hepatic or renal routes, in order to match the needs of the final clinical application.

The *in vivo* kinetic behavior of the agent is a key parameter in the application of radiolabeled antibodies for imaging or therapy. A balance must be found between exposure (to maximize signal for imaging or dose deposition for therapy) and clearance (to minimize background and normal tissue toxicity). A powerful approach has been the use of antibody fragments, produced enzymatically or through protein engineering. Antibodies can be reformatted into a variety of fragments, including smaller monovalent fragments such as single domain antibodies and scaffolds (Figure 1b), and monospecific and bivalent fragments such as minibodies and diabodies (Figure 1c). Additionally, antibody fragments

can be reformatted into more complex bispecific and bi- or multivalent fragments (Figure 1d), which may be applied for pretargeting (Figure 1e). Compared to intact antibodies, smaller fragments typically clear more rapidly from the circulation, resulting in higher contrast images at earlier times, and higher tumor-to-normal organ therapeutic (AUC) ratios. For imaging, antibody fragments that lack the Fc region are desired due to the removal of biological function and FcRn recycling, which allows for optimal contrast at shorter time points. Furthermore, reduction of the molecular weight of antibody-based agents to below ~60 kDa (the threshold for first-pass renal filtration) can dramatically accelerate clearance. For example, high contrast images can be obtained for small single-domain antibodies, scFvs or diabodies within the same day (4–8 hours), or for the larger minibody (scFv-C_H3) by the next day (24–48 hours), compared to intact antibody (1 week)[1]. For therapeutic applications, the circulation time of the radiolabeled antibody fragment needs to be sufficient for dose deposition in tumors, while limiting toxicity to normal tissues. The half-life of small fragments and scaffolds can be extended by chemical or recombinant approaches such as poly(ethylene glycol)-modification (PEGylation) or fusion to an Fc domain, albumin, or albumin-binding proteins[7]. Additionally, larger antibody fragments for RIT are typically above the renal filtration cutoff and are therefore cleared through the liver, which is more radioresistant compared to kidneys.

A growing spectrum of radionuclides are available for various applications including SPECT, PET, or RIT. Gamma and positron emitters are used for SPECT and PET, respectively, while applications using beta, alpha, and Auger emitters include targeted radiation therapy. The physical properties of the radionuclide, such as type of emission(s), decay energies, and half-life, are important to consider in matching an isotope with an antibody or antibody fragment. For imaging, the half-life of the radionuclide should ideally conform to the biological half-life of the antibody fragment. For therapy, the range of dose deposition and linear energy transfer (LET) are also important. Other considerations include conjugation and chelation strategy, residualization of the radionuclide, and practical concerns such as availability for research or clinical uses.

In this review we focus on protein engineering and its utilization for developing and optimizing antibody fragments for radionuclide delivery. Radionuclides commonly used for imaging and therapy are introduced, followed by a review of conjugation and radiolabeling strategies. Finally, this review summarizes recent advances in development of engineered antibodies and fragments ranging from single domain antibodies[8] to larger fragments[9], bispecific antibodies[10], and alternative scaffolds[11,12] for preclinical imaging, clinical imaging and radioimmunotherapy.

RADIONUCLIDES FOR IMAGING AND THERAPY

For both imaging and therapy, considerations for pairing a radionuclide with an antibody or fragment include half-life, conjugation chemistry and chelation strategy for radiometals, target internalization, and metabolism of the radiotracer (including residualization or efflux and elimination of radioactive metabolites). Radiometal-based probes are generally residualizing because radiometal-chelate metabolites are typically polar and charged, and therefore unable to diffuse through cell membranes[13]. These metabolites remain trapped in

the lysosomal compartment of cells, which can increase total uptake at target tumor tissues, but can also increase activity in normal tissue (particularly in organs of clearance). In contrast, antibodies radioiodinated using standard methodologies (i.e., using Iodogen) are internalized and metabolized to release free iodide or iodotyrosine, which readily efflux from the cell and are rapidly cleared from systemic circulation. The net result is reduced background in imaging, although overall activity at the target (tumor) tissue may also decrease over time due to internalization and processing. Residualizing radiometal-chelates or alternative iodination strategies may be more appropriate when targeting internalizing antigens, whereas nonresidualizing radiolabeling approaches may be preferred for antigens that remain on the cell surface. It is important to note that the process of internalization is not binary; there is a broad range in the rate and extent to which cell surface antigens can be internalized, from very rapid internalization (e.g., due to receptor cross-linking) to slow, physiological membrane turnover.

Common single-photon emitting radionuclides include ^{99m}Tc, ^{123}I, ^{131}I, and ^{111}In, and common positron-emitting radionuclides include ^{18}F, ^{68}Ga, ^{64}Cu, ^{89}Zr, and ^{124}I (Table 1). For immunoPET, shorter-lived radionuclides such as ^{18}F and ^{68}Ga can be used for same-day imaging and pair well with antibody fragments that have shorter biological half-lives, such as single domain antibodies, scFvs, or diabodies. Longer-lived radionuclides such as ^{64}Cu, ^{89}Zr and ^{124}I can pair well with the intact antibody or a larger antibody fragment, such as the minibody, for optimal imaging contrast 24–48 hours or later post-injection.

Other considerations for radionuclide selection for imaging include positron yield, range, and other co-emissions within the energy range of the scanner. For example, ^{68}Ga and ^{124}I have an increased positron range compared to ^{18}F which leads to decreased resolution and introduce additional partial volume effects (PVE) that can affect PET quantification[14]. Certain radionuclides, such as ^{64}Cu, also emit a high energy beta particle on decay, and thus act as both imaging and therapeutic agents. Other positron emitters can be used as a surrogate to estimate dosimetry of a therapeutic isotope, such as the pairing of the iodine isotopes ^{124}I and ^{131}I[15].

Radioimmunotherapy (RIT) enables specific delivery of the therapeutic radionuclide to the site of disease, although the long biological half-life of intact antibodies may result in dose to normal tissue[16]. Using an antibody fragment may be advantageous in limiting dosage to normal organs, especially radiosensitive tissues such as bone marrow; however, the kidney absorbed dose must be considered for fragment sizes that are excreted renally. Radionuclides for RIT emit beta, alpha, or Auger electrons (Table 2), and cause cytotoxic DNA damage by numerous mechanisms including via reactive oxygen species, single and double stranded breaks, and inhibition of DNA damage repair mechanisms[17,18]. Independent of the radionuclide, cell death can also be caused by an immune response such as antibody-dependent cellular cytotoxicity, but the protein mass used in RIT is typically much lower than a conventional therapeutic antibody dose. The choice of radionuclide depends on a multitude of factors, including the type and size of cancer being targeted, target density, and heterogeneity, as the beta, alpha, and Auger particle emissions vary in range and LET.

Beta-emitting radionuclides for RIT have a low LET (0.2 keV/mm) and a relatively long range in tissue (one to several mm), and they can therefore damage tissue throughout the tumor, as well as adjacent normal tissue, due to cross-fire and radiation field effect across several millimeters (Figure 2). Common beta emitters include ^{131}I, which is readily available and has long been used for thyroid cancer treatment. Both ^{131}I and ^{177}Lu co-emit a gamma photon that can be detected by SPECT imaging that can complement RIT. Conjugated antibodies radiolabeled with ^{177}Lu and ^{90}Y are catabolized to yield charged radiometal chelate metabolites that residualize in tumor cells for increased tumor retention. A disadvantage of ^{90}Y is it emits almost exclusively beta particles and cannot be imaged by conventional methods; however, ^{90}Y produces bremsstrahlung photons and Cerenkov radiation which can be detected by SPECT and by optical Cerenkov luminescence imaging, respectively[19]. Alpha emitters have a much shorter range (a few cell diameters) and a high LET (80–100 keV/μm), and they can be effective for smaller lesions and metastases (Figure 2). Alpha emitters commonly used in RIT studies include ^{213}Bi, ^{223}Ra, the radiohalogen ^{211}At, and the radiometal ^{225}Ac[20. ^{225}Ac decays into four alpha-emitting daughter particles, two of which emit an imageable gamma ray, and ^{225}Ac-radiolabeled full length antibodies have been efficacious in tumor-cell killing in *in vitro* and *in vivo* preclinical studies[21,22], as well as clinical studies[3,23]. Auger emitters, such as ^{125}I, have low energy and are considered to have high LET (4–26 keV/μm) with a very short path length of 2–500 nm[24] (Figure 2). Similar to alpha emitters, Auger emitters may be more suitable for limiting damage to normal tissues compared to beta-emitters[25]; however, strategies must be devised for intracellular delivery, preferably in the vicinity of the cell nucleus.

Other radiometals to consider for antibody-mediated imaging and therapy include ^{47}Sc, ^{67}Cu, ^{149}Tb, ^{161}Tb, ^{166}Ho, and ^{212}Pb[21] (Table 1). Some of these radionuclides emit both beta particles and gamma rays useful for therapy and imaging (^{47}Sc, ^{67}Cu, and ^{166}Ho). ^{149}Tb emits alpha particles, positrons, and imageable gammas, and therefore may also be used for therapy and imaging by SPECT or PET. Although these radionuclides have primarily been used to label full-length antibodies for therapy, they have been successful in preclinical and clinical trials and could be explored as effective radiolabels for antibody fragment-based RIT[21].

LABELING STRATEGIES

Antibodies can be engineered to optimize conjugation and labeling, and radiolabeling strategies depend on the physics and chemistry of the radionuclide. Radioiodine is commonly used for both imaging and therapy, and radioiodination can be achieved by directly radiolabeling the iodine radioisotope to tyrosines on the antibody or antibody fragment using well-established procedures[26]. Although radioiodine is nonresidualizing, methods have been established to maximize retention in lysosomes such as using the aromatic N-succinimidyl 4-guanidinomethyl-3-iodobenzoate (SGMIB)[27].

In contrast with direct radiodination, radiometal labeling requires a chelator, and a wide variety of bifunctional acyclic and macrocyclic chelators have been developed[28,29]. A common acyclic chelator is diethylenetriaminepentaacetic acid (DTPA), and its derivative trans-(S,S)-cyclohexane-DTPA (CHX-A”-DTPA) may be used to achieve high radiolabeling

efficiency with less influence from competing trace metal ions, as shown in a comparison study chelating ^{177}Lu and ^{111}In[30,31]. The acyclic chelator desferrioxamine (DFO) is typically used with ^{89}Zr due to its more complex coordination chemistry[32], as well as ease of radiolabeling without necessitating working in metal-free conditions[33]. Although acyclic chelators result in high radiolabeling efficiency, macrocyclic chelators provide greater thermodynamic and kinetic stability[34]. Cyclic chelators include 1,4,7,10-tetraazacyclododecane-1,4,7,10-tetraacetic acid (DOTA), 1,4,7-triazacyclononane-N,N′,N″-triacetic acid (NOTA), and 1,4,8,11-tetraazacyclododecane-1,4,8,11-tetraacetic acid (TETA). DOTA has four chelating carboxylates and four nitrogens, and it is used to chelate radiolabels such as ^{111}In, ^{177}Lu and ^{90}Y. NOTA has a smaller ring structure with three carboxylates and nitrogens, and it is preferred for ^{64}Cu and ^{68}Ga due to superior binding.

Antibodies can be conjugated to chelators typically by N-hydroxysuccinimide (NHS) or isothiocyanate (SCN) chemistry, which react with the ε–amino group of lysines on the antibody and require alkaline conditions (pH 7.2–9). Sortase-mediated reactions can be used for N-terminal or C-terminal site-specific labeling[35]. For example, a protein modified with Leu-Pro-Xxx-Thr-Gly motif will be recognized by sortase A, which catalyzes the transpeptidation reaction that allows for the addition of a moiety with N-terminal glycine residues. Thiol-labeling strategies can also be used to conjugate chelators to solvent-exposed cysteines. An engineered C-terminal cysteine can be used for site-specific labeling, which is advantageous to control the conjugate-to-antibody ratio, improve the homogeneity of the product, and direct the radiolabel away from binding sites. Maleimide chemistry is the most widely used strategy for site-specific labeling thiols, and the reaction can occur at pH 7 which is favorable for antibodies. However, maleimide-thiol modification can be unstable *in vivo*; therefore, other thiol-labeling strategies have been explored including employing phenyloxadiazole sulfones, dibromomaleimides, and dithiophenolmaleimides[36].

Conventional strategies to label proteins with ^{18}F involve a multi-step process using prosthetic groups such as amine reactive N-succinimidyl 4-[^{18}F]fluorobenzoate ([^{18}F]SFB), as direct fluorination is typically unfeasible due to the harsh conditions required[37]. Newer labeling methods have been developed to simplify the process, such as automated syntheses or applying microfluidic technology. For example, [^{18}F]SFB labeling was adapted for use via a microfluidic chip, and this method successfully labeled a cys-diabody used for immunoPET imaging in preclinical tumor models[38]. Thiol-reactive maleimide-based prosthetic groups can also be employed, such as *N*-[2-(4-[^{18}F]fluorobenzamido)ethyl]maleimide ([^{18}F]FBEM), which has been used to label an Affibody™ (Affibody AB; see below) for PET imaging[39]. Another approach involves [^{18}F]fluoride acceptors, such as Al^{18}F that can be complexed with NOTA-conjugated moieties[40] such as haptens for pretargeted imaging, or antibody fragments and scaffolds[41]. Lastly, bio-orthogonal click chemistry is a powerful method for rapid fluorination, which is critical due to the short half-life of ^{18}F.

Bio-orthogonal click chemistry is enabled by engineering strategies such as introducing cysteine residues or unnatural amino acids. Click reactions include copper-free strain-promoted Huisgen cycloaddition and inverse-electron-demand Diels-Alder reaction between tetrazine (Tz) and transcyclooctene (TCO)[42]. Bioorthogonal click reactions allow for rapid

radiolabeling (10–15 minutes)[42], which is advantageous especially for using radionuclides with short half-lives such as ^{18}F. The bioorthogonal click reaction between Tz and TCO has been used for both pretargeted ^{18}F-PET imaging[43 and 64]Cu-PET imaging[44,45] of *in vivo* models, resulting in high contrast images. Additionally, click chemistry between Tz and TCO has also been applied to conjugate the two arms of an anti-EGFR and anti-CD105 bispecific antibody, which was subsequently used for PET imaging[46]. Lastly, click chemistry has been applied for pretargeted radioimmunotherapy studies with TCO-modified anti-CA19.9 and ^{177}Lu-Tz radioligand[47].

INTACT ANTIBODIES IN THE CLINIC

Intact antibodies continue to provide clinical use as therapeutics, and recent approvals of antibodies include avelumab and atezolizumab (anti-PD-L1), inotuzumab (anti-CD22), sarilumab, dupilumab, and brodalumab (anti-IL-6, IL-4, and IL-17 receptors, respectively), as well as several others for cancer and non-cancer targets[48]. Many of these approved antibodies are candidates for labeling for immunoPET, which can assess the status of the target, inform whether the patient is a good candidate for the therapy, and allow for therapy personalization[49]. For example, ^{89}Zr-trastuzumab was used to detect unsuspected HER-positive metastases in HER-negative patients[50], and the diagnostic potential was also evaluated in comparison with 2-deoxy-2-[^{18}F]fluoro-D-glucose (^{18}F-FDG) PET imaging (NCT01420146). ^{89}Zr-trastuzumab is currently being evaluated to identify patients that may not respond to HER2 treatment T-DM1 (NCT01565200), while a first-in-human ^{89}Zr-pertuzumab imaging study in HER2-positive patients showed successful targeting of lesions including brain metastases[51]. Other immunoPET clinical trials include evaluation of ^{89}Zr-rituximab imaging in patients with immune-mediated inflammatory diseases of the lung (NCT02251964), ^{89}Zr-pembrolizumab in patients with non-small-cell lung cancer (NCT03065764), ^{89}Zr-ipiliumumab in treated patients with metastatic melanoma to assess uptake and correlation between tumor targeting and therapy response (NCT03313323), and ^{89}Zr-atezolizumab to monitor breast, bladder, non-small cell lung patients receiving atezolizumab therapy.

In addition to ^{89}Zr-based immunoPET, pilot clinical trials are currently evaluating ^{64}Cu- and ^{124}I-labeled antibodies. Examples include evaluation of the diagnostic imaging agents ^{64}Cu-M5A in patients with CEA-positive cancer (NCT02293954), ^{64}Cu-trastuzumab to predict response to trastuzumab or pertuzumab in patients with HER2-positive breast cancer (NCT02827877), and CD38-directed ^{64}Cu-daratumumab in patients with recurrent multiple myeloma. Additionally, comparison between standard CT and ^{124}I-cG250 immunoPET, which targets tumor-associated carbonic anhydrase isoenzyme IX, is being tested in patients with clear cell renal cell carcinoma to predict response to sunitinib or pazopanib treatment (NCT01582204). Lastly, a Phase I trial is testing ^{124}I-859 as a therapeutic to treat children with diffuse intrinsic pontine glioma using convection-enhanced delivery, where the brain tumor is directly infused the agent (NCT01502917).

Although only two radioimmunotherapy agents have been approved by the FDA, ibritumomab tiuxetan (Zevalin®) and tositumomab (Bexxar®), numerous intact antibodies for RIT are currently under clinical investigation. Recent studies include Phase I study of

^{131}I-8H9 targeting B7-H3 in patients with intraperitoneal tumors (NCT01099644), and a Phase III study of Iomab-B (^{131}I-anti-CD45 BC8) to condition patients with acute myeloid leukemia for bone marrow transplant (NCT02665065). Additional investigations include a Phase I trial of ^{177}Lu-5B1 treatment of CA19-9 positive cancers such as pancreatic adenocarcinoma (NCT03118349), a Phase I/II study evaluating ^{177}Lu-Lilotomab (Betalutin®) in patients with relapsed Non-Hodgkin Lymphoma (NCT01796171), and a Phase III comparison between ^{90}Y-ibritumomab tiuxetan (Zevalin®) and autologous stem cell transplantation in patients with follicular lymphoma (NCT01827605). Evaluation of alpha-emitter-based RIT includes a Phase I/II trial to test ^{211}At-BC8-B10 to target cancerous cells before blood stem cell transplant in patients with leukemia (NCT03128034), Phase I study of ^{227}Th-anti-CD22 (BAY1862864) in patients with Non-Hodgkin Lymphoma (NCT02581878), and Phase I study of ^{225}Ac-lintuzumab targeting CD33 in patients with refractory multiple myeloma (NCT02998047), and in older acute myeloid leukemia patients (NCT02575963). Many of these studies target lymphoma and leukemia cancers due to their radiosensitivity[3], yet there is potential for RIT to treat solid tumors as well. While intact antibodies have been highly effective agents for radionuclide delivery, the following sections will focus on antibody fragments.

ENGINEERING ANTIBODY FRAGMENTS: ASSEMBLING THE PUZZLE PIECES

By assembling knowledge of radionuclides, chemistry and labeling strategies with engineered antibodies, fragments, and scaffolds, novel agents have been developed for oncological and immune oncological applications. Strategies to achieve optimal high-contrast images or therapeutic effect include comparison of multiple fragment formats or radionuclides, and using bispecific antibodies and radiolabeled haptens for pretargeting. Here, we highlight recent studies that investigate engineered antibodies for oncological targets such as markers expressed in breast, prostate, and brain cancer, as well immune cell subsets. The antibody fragments discussed are the single-domain antibody, diabody, minibody, bispecific fragments, and alternative scaffolds (Figure 1).

Overview

Single-domain Antibody—Single-domain antibodies (sdAb, 12–15 kDa) (Figure 1b) include small monomeric fragments derived from human variable domains V_H or V_L, camelid heavy chain V_HH (also indicated as VHH), and shark heavy chain V_{NAR}. These sdAbs have high stability and low immunogenicity, and their small size and more compact structure can allow for better targeting compared to conventional antibodies[8]. The camelid and shark domains have long CDR3 regions, which allow for improved extension into cavities of target antigens[52]. More recent radiolabeled sdAb studies have focused on the camelid V_HH (Nanobody, registered trademark of Ablynx NV), and common targets include PSMA[53], CEA[54], and EGFR[55], HER2[56–60], and immune cell markers[61,62].

Diabody—The diabody is a noncovalent scFv dimer (~55 kDa) in which a shortened linker prevents the V_H and V_L from self-pairing, forcing cross-pairs in trans with a second chain to form a dimer, reconstituting two binding sites[63] (Figure 1c). Radiolabeled diabodies have

been successfully used for high-contrast PET imaging of a variety of targets due to improved tumor penetration compared to intact antibody, and the fast clearance of the diabody with a serum half-life of 2–5 hours is advantageous for same-day PET imaging of immune cell subsets, such as CD20 B[64] and CD4 and CD8 T cells[65–67], as well as solid tumors, including prostate cancer[68]. These studies have used diabodies radiolabeled with ^{18}F for same-day imaging or longer-lived radionuclides, such as ^{124}I and ^{89}Zr, for next-day imaging.

Minibody—The minibody is a bivalent dimer comprising of a scFv with a human gamma 1 hinge and C_H3 (~80 kDa) (Figure 1c) with a serum half-life of 5–12 hours, and the size directs clearance to the liver. Radiolabeled minibodies have been effective as diagnostic PET imaging tracers targeting CEA[69,70], CD8 T cells[71], CD20 B Cells, PSCA[72,73], and PSMA[74], and high tumor-to-blood ratios can typically be achieved by 24–48 hours post-injection[75]. Small immunoproteins (SIPs) are recombinant proteins similar to the minibody composed of scFv dimerized by the C_H4 domain of IgE heavy chains, and they have demonstrated success as RIT agents[76–79]. Preclinical and clinical studies have demonstrated the effectiveness of using the minibody for earlier lesion detection compared to intact antibody.

Bispecific Antibodies for Pretargeting—Antibody engineering enables novel functionality such as bispecific binding. Bispecific antibodies (bsAbs) (Figure 1d) can target two or more antigens and may improve delivery to a tumor for better imaging or therapeutic outcome. Many bispecific formats have been engineered for a variety of diagnostic and therapeutic applications, and the engineering techniques used to generate these various formats as well as their clinical development have been recently reviewed[80,81]. BsAbs typically are used to bring two targets together, such as two ligands for inactivation, or a tumor antigen and T cell antigen in order to achieve a T-cell mediated therapeutic effect. For example, blinatumomab is a bispecific T-cell engager (BiTE) that targets CD19 on B cells and CD3 on T cells, resulting in T cell activation to respond to B cell malignancies, specifically acute lymphoblastic leukemia[82]. Dual-affinity retargeting (DART) bispecifics can also bind two targets for improved potency, such as the CD19 × CD3 MGD011 shown to induce tumor regression in B-cell lymphoma and leukemia models[83]. Additionally, several non-oncology bispecifics are also currently in development[84].

BsAbs can be particularly useful for radionuclide delivery as part of a pretargeting strategy. In this approach, one arm of the bispecific targets the tumor, and the other arm recognizes a radiolabeled hapten (typically a small molecule or peptide) for imaging or RIT (Figure 1e). The bsAb is first administered and allowed to accumulate in the tumor, with sufficient time to clear from the circulation. Subsequently, the radiolabeled hapten is injected, which rapidly binds to the pre-localized antibody[85]. Another effective pretargeting strategy uses a trivalent bsAb with two target-specific Fabs and an anti-histamine-succinyl-glycine (HSG) Fab, and the three arms of this Tri-Fab (TF) are linked by disulfide bonds. Example targets for bispecific antibody pretargeting include CD105 and EGFR[46], CEA[86,87], and TROP2[88].

Alternative Protein Scaffolds—A wide range of antibody-like small protein scaffolds are currently in development as drugs for diseases such as cancers, atherosclerosis, and macular degeneration, as described in a recent review[12]. These scaffolds are easy to produce in bacteria or yeast and are typically stable in harsh labeling conditions such as high

temperature. They range from 2 to 20 kDa, which enables tissue penetration to access binding sites more easily than intact antibodies. However, the small size also results in fast renal filtration, and certain applications may require engineering or other modifications to increase the half-life. For example, PEGylation, Fc fusion, albumin fusion, or use of albumin binding domains can extend the half-life of antibody fragments.

A widely explored scaffold for radionuclide delivery is the Affibody (registered trademark of Affibody AB), small (6.5 kDa) scaffolds composed of alpha helices originally based on the Z domain of staphylococcal protein A[89]. Affibody protein scaffolds have high affinity and specificity, as well as the ability to tolerate harsh labeling conditions without impacting binding. Affibodies rapidly penetrate tumors for early high-contrast images due to rapid extravasation and tumor penetration[90], and they are compatible with short-lived radionuclides such as ^{68}Ga and ^{18}F for PET, or ^{11}In for SPECT. Affibody-based imaging and therapy have been developed to target EGFR[91,92] and HER2[93–98], which has been successful in preclinical and clinical studies.

Preclinical imaging studies

Single-domain Antibody—SdAb-based immunoPET has been used to monitor immune responses. One group developed VHHs targeting CD11b (VHHDC13) and class II MHC (VHH7), which are expressed on a variety of myeloid cells that often locate to tumor margins and can provide information on treatment response[61]. Site-specific ^{18}F radiolabeling was achieved using a two-step click tetrazine/transcyclooctene (TCO) and sortase-catalyzed modification, and ^{18}F-VHH7 and DC13 successfully detected tumor-associated macrophages and other activated myeloid cells in human melanoma xenograft models (Figure 3a). ImmunoPET imaging was also used to monitor CD8+ T cells using ^{89}Zr-PEGylated-anti-CD8 VHH, and 5, 10, and 20 kDa PEG moieties were tested to improve the pharmacokinetics of the nanobody[62]. Epithelial cell adhesion marker (EpCAM) expression was used to sort epithelial (EpCAM-high) and mesenchymal-like (EpCAM-low) carcinoma cells, which were implanted into mice that received anti-CTLA4 or no treatment, and tumors were assessed for immune cell infiltration by ^{89}Zr-PEGylated VHH-X118. Mice bearing EpCAM-high well-differentiated tumors with homogenous activity in the tumor responded to the treatment, while EpCAM-low mesenchymal tumors with heterogeneous activity correlated with poor response.

Macrophage mannose receptor (MMR) has also been targeted by camelid VHH-based sdAbs in order to image tumor-associated macrophages (TAMs) *in vivo.* ^{99m}Tc-3.49-anti-MMR sdAb were shown to target pro-angiogenic TAMs in mice, and co-injecting unlabeled bivalent sdAb helped decreased nonspecific background while preserving tumor uptake[99]. Due to the success of the anti-murine MMR sdAb, cross-reactive anti-mouse/human MMR sdAbs were generated for future clinical translation[100]. 3.49-sdAb was labeled with [^{18}F]SFB for PET in mouse tumor models. In contrast to using ^{99m}Tc, ^{18}F-3.49-sdAb resulted in a 20-fold decrease in kidney uptake, and therefore ^{18}F is the preferred radiolabel. Because MMR is highly expressed in TAMs correlating with more advanced tumor stage, this sdAb could inform prognosis of solid tumors.

HER2 expression is important to assess in breast cancer patients in order to determine if they can benefit from HER2-targeted therapies. One study assessed HER2 expression in BT474M1 human breast carcinoma xenografts by PET imaging using 5F7 anti-HER2 Nanobody radiolabeled with ^{18}F, which pair well due to similar short biological and physical half-lives (1–2 h and 1.8 h, respectively)[56]. The authors describe a novel residualizing labeling strategy based on N-succinimidyl 4-guanidinomethyl-3-iodobenzoate (SGMIB) (^{18}F-RL-I-5F7), which resulted in higher tumor accumulation and retention compared to nonresidualizing [^{18}F]SFB-5F7, and had comparable results with ^{18}F-anti-HER Affibodies. However, 5F7 binds to the same epitope as trastuzumab, and therefore a similar study was conducted using ^{18}F-anti-HER2 Nanobody 2Rs15d[57]. 2Rs15d does not compete with trastuzumab and pertuzumab binding domains and therefore may be preferred for clinical use in patients receiving those therapies.

These studies demonstrate how sdAbs are advantageous due to the rapid elimination resulting in high contrast images as early as 1 hour post-injection, and kinetics that enable the use of radionuclides with short half-lives such as ^{18}F and ^{68}Ga. SdAbs can penetrate tumors more effectively than full-length antibodies, and their preclinical success has led to several clinical trials.

Diabody—The short serum half-life of diabodies in mice enables the use of radionuclides such as ^{18}F for same-day imaging, as demonstrated with [^{18}F]SFB-T84.66 anti-carcinoembryonic antigen (CEA) diabody in mice bearing LS 174T human colon carcinoma tumors[101]. Some studies have compared radiolabeled diabodies with other fragment sizes, such as minibody, intact antibody, triabody, and Fab′ to determine the optimal fragment for PET imaging[102,103]. While there may not be a single clear choice, the optimal fragment or fragments can differ study to study depending on variables such as the model and preferred route of clearance. For example, the ^{18}F-anti-carcinoembryonic antigen (CEA) monoclonal antibody hMN-14 (labetuzumab) derivatives hMN-14-Fab′, hMN-Fab-AD2, and hMN-diabody were assessed in a comparison study[102]. All derivatives showed specific uptake in LS174T xenografts compared to CEA-negative xenografts; however, the diabody showed higher liver activity that may obscure liver metastases in future models, and further modification would be made to reduce hepatic uptake. On the other hand, ^{68}Ga-labeled diabody or scFv administered to mice bearing EpCAM-expressing A-431 tumors had optimal tumor-to-organ ratios at early time points compared to triabody, and IgG, and the results support using the diabody for ^{68}Ga-based imaging of solid tumors[103].

Engineered diabodies have been used for SPECT and PET imaging of solid tumors, such as prostate cancer. The humanized intact antibody J591 targeting prostate specific membrane antigen (PSMA) was modified to a diabody with a C-terminal cysteine (J591Cdia) to form a more stable dimer[104]. ^{99m}Tc-J591dia was used for same-day SPECT imaging of mice bearing subcutaneous PSMA-positive prostate carcinoma tumors, and specificity was confirmed through blocking studies. J591 derivatives for PET imaging include cysteine diabody and minibody, which were radiolabeled with ^{89}Zr and demonstrated rapid tumor targeting in mice bearing PSMA-positive xenografts[68]. The advantages of using these fragments in comparison with ^{89}Zr-intact J591 are lower dose toxicity due to shortened residence time, which would be especially important in patients requiring repetitive imaging

to monitor treatment response. J591-based anti-PSMA cys-diabody has also been used to direct chemotherapy-loaded lipid nanoparticles (LNP) as a strategy to improve tumor accumulation[105]. The diabody-targeted LNPs were radiolabeled with ^{64}Cu and shown by PET to increase tumor targeting and decrease drug clearance in a PSMA prostate cancer.

Engineering a cys-diabody (cDb) with a C-terminal cysteine can also allow for site-specific conjugation and radiolabeling, as exemplified in several immunoPET studies targeting immune cell subsets[64–67]. In a study targeting B cells for immunoPET, obinutuzumab-based GA101 cDb and cys-minibody (cMb) tracers were evaluated in mice bearing human CD20-expressing lymphoma xenografts as well as in transgenic mice expressing huCD20 (huCD20 TG) on normal B cells[64]. These humanized type II tracers bind to CD20 in a different orientation than type I antibodies such as rituximab, the standard therapy for lymphoma patients, and were shown to outperform rituximab-based fragment imaging. Nonresidualizing ^{124}I was compared with residualizing ^{89}Zr-labeled antibody fragments to assess the modulation of CD20, which was shown to internalize in huCD20 TG B cells more rapidly than in CD20 lymphoma cells.

Cys-diabodies have also been developed to image the T cell compartment. Anti-CD4 GK1.5 and anti-CD8 2.43 cDbs were generated to detect helper/regulatory and cytotoxic T cells by immunoPET, and they were successfully used to monitor T cell repopulation in a hematopoietic stem cell transplantation model[65]. Anti-CD4 GK1.5 cDb was shown to decrease CD4 expression and inhibit proliferation in a dose-dependent manner *in vivo,* and low protein dose was determined to be ideal for obtaining high contrast immunoPET images for future imaging studies[66]. Detecting these immune cell subsets can be especially powerful to monitor therapy response, such as a preclinical study using ^{89}Zr-anti-CD8 169 cDb to track changes in tumor-infiltrating and systemic CD8 expression in several immunotherapy models (Figure 3b)[67]. In CT26 tumor-bearing mice that received anti-CD137/4-1BB immunotherapy, ^{89}Zr-169 cDb detected tumor infiltrating T cells in the treated group compared to untreated or CD8-blocked mice. In another immunotherapy model, 25 to 33% of mice bearing CT26 xenografts were previously reported to respond to anti-PD-1 or anti-PD-L1 checkpoint blockade therapy. Mice received anti-PD-L1 therapy and were grouped into responders and nonresponders. ^{89}Zr-169 cDb PET imaging detected tumor-infiltrating CD8+ T cells in responders compared to nonresponders, confirmed by *ex vivo* biodistribution, and transverse images of responders show intratumoral activity while nonresponders show a peripheral rim of activity (Figure 3a). The ability to detect CD8+ T cells in these two immunotherapy models support future clinical studies using immunoPET to monitor the tumor immune microenvironment and response to therapy.

Minibody—The anti-CEA T84.66 minibody (Mb) and diabody (Db) fragments have been radiolabeled with ^{111}In or ^{125}I/^{131}I for radioimmunoscintigraphy and biodistribution comparison in murine models[70]. The T84.66 Db demonstrated rapid tumor targeting, although the ^{111}In- T84.66 Db displayed high renal uptake. On the other hand, as expected, the minibody exhibited low renal uptake but higher hepatic uptake, which might limit imaging and therapy of CEA-positive hepatic disease. In comparison, the radioiodinated fragments cleared more quickly, and was favored due to reduced nonspecific background. These studies demonstrate tumor targeting and clearance should be assessed in choosing a

favorable radionuclide depending on the disease setting. ^{124}I-T84.66 Mb was used for successful PET imaging of mice bearing human LS174T colon carcinoma xenografts, and small CEA-positive tumors less than 3 mm in diameter could be detected[69].

^{123}I-cT84.66 chimeric minibody was assessed in a pilot clinical trial in patients with colorectal cancer[106]. Eight of ten tumors larger than 1.0 cm were successfully imaged by SPECT, compared to five of ten detected by CT. However, the mean residence time of the minibody is longer than the short half-life of ^{123}I (13 h), and a radionuclide with a longer half-life such as ^{124}I, or residualizing properties such as ^{89}Zr, may be more suitable for future clinical studies.

As discussed in the previous section on diabodies, engineered antibody fragments have been developed for immunoPET of T and B cells. Two allele-specific murine anti-CD8 minibodies were developed, 2.43 Mb targeting the CD8α isoform Lyt2.2 Mb in BL/6 mice and 169 Mb that binds CD8α in all mouse strains[71. 64]Cu-NOTA-2.43 and 169 Mbs were used to obtain high-contrast PET images at 4 h post-injection, and ^{64}Cu-NOTA-2.43 Mb specificity was shown through both blocking and depleting studies. In comparative studies discussed in the previous diabody section using B-cell lymphoma models, ^{124}I-anti-CD20 GA101 cMb resulted in higher tumor accumulation compared to ^{124}I-rituximab cMb (RxcMb) in mice bearing s.c. 38C13-huCD20 tumors[64]. Interestingly, higher tumor retention was reached despite obinutuzumab (type II binding) only binding half of the surface density compared to rituximab (type I binding), which was postulated to be due to rituximab's faster off-rate. In human CD20 transgenic mice, ^{89}Zr-GA101 cMb successfully detected lymph nodes and showed specific uptake in the spleen[64]. The evaluation of both GA101 cDb and cMb offers optimized PET tracers for future studies to understand the modulation of CD20 in response to antibody-based therapies such as rituximab. These immune cell-targeted minibody tracers can be useful for studying preclinical disease models in mice, such as immune cell infiltration in tumor models, or predicting or monitoring response to therapy.

Minibodies have also been used for preclinical PET imaging of prostate cancer targets including human prostate stem cell antigen (PSCA)[73] and PSMA[68. ^{124}]I-A11 Mb and ^{89}Zr-A11 Mb immunoPET were compared, and ^{124}I-A11 Mb resulted in superior tumor-to-soft tissue contrast in mice bearing 22Rv1-PSCA human prostate carcinoma xenografts[73]. The longer positron range of ^{124}I and ^{89}Zr influences resolution, and therefore partial-volume correction was applied to improve *ex vivo* quantification. ^{124}I-A11 Mb PET was also applied to a intratibial tumor model representing bone metastasis and successfully detected intratibial xenografts with higher sensitivity and specificity than ^{18}F-Fluoride bone scans[72]. Additionally, decreased tumor uptake of ^{124}I-A11 Mb in response to enzalutamide treatment corresponded with PSCA downregulation, and was detectable before the tumor volume changed. ImmunoPET of PSCA may be explored for clinical translation to monitor response to androgen deprivation therapy.

Bispecific Antibodies for Pretargeting—A bispecific antibody composed of an anti-epidermal growth factor receptor (EGFR) Fab and anti-CD105 Fab was generated by biorthogonal click chemistry[46]. This Bs-F(ab)$_2$ was radiolabeled with ^{64}Cu and used for immunoPET to detect s.c. U87MG human glioma tumors in mice, demonstrating high

sensitivity even in small 3 mm tumors. Additional near-infrared fluorescence imaging with ZW-800 provided proof-of-principle for image-guided surgical resection. A similar click chemistry approach was used to assemble bispecific anti-CD105 Fab × anti-tissue factor (TF) Fab fragments, and ^{64}Cu-NOTA-heterodimer-ZW800 visualized s.c. pancreatic tumors by dual-modality PET/NIRF imaging[107]. Compared with blocked CD105 or TF, the dual-targeting approach resulted in increased tumor targeting. These preclinical studies support the use of bispecific antibodies for more enhanced tumor signal, and other studies could use this method to monitor therapy by bispecific targeting a tumor antigen and T cells.

Alternative Protein Scaffolds—In one study, an agouti-related protein (AgRP) cystine knot mutant (4 kDa) was developed to bind $\alpha_v\beta_3$ integrin with high affinity for PET imaging[108]. The cysteine knot has a core composed of three or more disulfide bonds that are interwoven, and this highly stable scaffold can tolerate high temperatures. ^{64}Cu-DOTA-AgRP-7C was administered to mice bearing U87MG glioblastoma xenografts that express the $\alpha_v\beta_3$ integrin, and high contrast PET images were obtained by 1–2 hours post-injection. The authors discussed strategies to improve pharmacokinetics in future studies, including engineering prosthetic groups to increase tumor targeting or co-injecting cationic amino acids such as lysine to decrease the high kidney uptake, which can also be applied to small fragments such as diabodies.

The Affibody has been used to target epidermal growth factor receptor (EGFR) for SPECT imaging in murine xenografts, as well as EGFR-specific fluorescent imaging in human skin epidermoid carcinoma and human glioma xenografts[90]. The following studies are based on the anti-HER2 Affibody $Z_{HER2:342}$. The $Z_{HER2:342}$ was affinity matured to picomolar affinity and successfully used for preclinical imaging of HER2+ xenografts[91]. Compared to ^{124}I-trastuzumab, ^{124}I- $Z_{HER2:342}$ provided higher contrast images at earlier time points, demonstrating its use as an imaging tool to assess changes in HER2 expression[92]. Affibody molecules have also been developed targeting HER3 as shown in several preclinical models[109,110]. A number of affibodies are in development for other medical applications such as fluorescent-guided surgery or as therapeutic drugs[109], and these molecules may also be radiolabeled in future studies evaluating their potential as diagnostic imaging agents.

Clinical Imaging Studies

Single-domain antibody—The first-in-human application of a radiolabeled Nanobody was a Phase I clinical trial testing the biodistribution and HER2-positive tumor-targeting of ^{68}Ga-2Rs15d in 20 patients (Figure 4a)[59]. The resulting PET images showed a wide range of tumor uptake and low background activity, and it was hypothesized that this application would be useful for HER expression assessment especially in cases of metastatic breast cancer.

Clinical trials using single-domain antibodies include the evaluation of ^{131}I-SGMIB anti-HER2 VHH1 dosimetry for RIT and tumor imaging in breast cancer patients (NCT02683083), ^{68}Ga-NOTA-anti-HER2 VHH to detect brain metastases in breast cancer patients (NCT03331601), and ^{99m}Tc anti-PD-L1 VHH for SPECT/CT of non-small cell lung cancer (NCT02978196).

Minibody—In a comparison study of ^{89}Zr-anti-PSMA J591 antibody fragments, the minibody IAB2M resulted in higher tumor uptake than the diabody and faster clearance than the intact antibody in preclinical prostate cancer models[68], and therefore it was developed further in the clinic. ^{89}Zr-IAB2M demonstrated success in the following Phase I first-in human study, which assessed dose escalation of the minibody in eighteen patients with metastatic prostate cancer[74]. ^{89}Zr-IAB2M PET targeted bone and soft tissues lesions in 17 of 18 patients by 48 hours, compared to baseline ^{99m}Tc-MDP (9 patients) or CT (6 patients) to detect bone lesions, or MRI (14 patients) or ^{18}F-FDG-PET (10 patients) to detect nodes or soft tissue lesions (Figure 4b). The highest uptake was observed in patients who received 10 mg, compared to 20 and 50 mg, which was determined to be the optimal protein dose for imaging. Compared to PSMA-targeting peptides, little to no uptake was observed in lacrimal and salivary glands, increased uptake over time was observed in the gastrointestinal tract (small intestine, 0.36 ± 0.06 mGy/MBq) and kidney (1.36 ± 0.26 mGy/MBq), and liver uptake (1.67 ± 0.3 mGy/MBq) was attributed to minibody clearance and residualizing radiometal.

Radiolabeled minibodies tested in clinical trials include the current Phase I trial evaluating ^{89}Zr-Df-IAB22M2C, which targets CD8 T cells, in patients with metastatic solid malignancies or Hodgkin's lymphoma (NCT03107663). ^{89}Zr-Df-IAB2M anti-PSMA minibody has also been expanded to a Phase I/IIa trial in patients with metastatic prostate cancer (NCT01923727).

Bispecific antibodies for pretargeting—A first-in-human study was conducted using TF2 and ^{68}Ga-IMP288 pretargeting for PET imaging of patients with metastatic medullary thyroid carcinoma (MTC), and high-contrast images were obtained with a preferred pretargeting delay of 30 hours (Figure 4c)[111]. Due to the consistent expression of CEA independent of prognosis in MTC, this target could provide more information independent of changes in disease state compared to ^{18}F-FDG or L-3,4-dihydroxy-6-[^{18}F]fluorophenylalanine (^{18}F-DOPA). Anti-CEA TF2 and ^{68}Ga-IMP288 PET imaging was also evaluated in patients with metastatic colorectal cancer (NCT02587247) and breast carcinoma (NCT01730612).

Alternative scaffolds—Clinical studies using radiolabeled ABY-002 and ABY-025 have successfully visualized HER2-positive lesions[109]. The first-in human Affibody, ABY-002, is a second generation derivative of $Z_{HER2:342}$ and was used for SPECT and PET imaging. ^{111}In-ABY-002 and ^{68}Ga-ABY-002 successfully detected metastases in patients with recurrent breast cancer[93]. The Affibody ABY-025 was reengineered to target an epitope separate than the epitopes (HER2) targeted by therapeutics in order to enable imaging during therapy. ^{111}In-ABY-025 first-in-human studies successfully assessed HER2 status in metastatic breast cancer patients, and the SPECT images additionally showed a difference in uptake between HER2+ and HER2- metastases[94]. Subsequent phase I/II studies used ^{68}Ga-ABY-025 PET imaging to determine whole-body HER2 expression (Figure 4d)[95].

Radioimmunotherapy studies

Single-domain antibody—The Nanobody 2Rs15d targeting HER2 has also been evaluated in theranostic studies. ^{177}Lu-DTPA-2Rs15d was injected in mice bearing SKOV3-LUC (Luciferase^{pos}) xenografts, and by day 125 tumor growth was halted with 5 of 8 mice completely tumor-free and 3 of 8 mice bearing unpalpable LUC^{pos} tumors[58]. The authors co-injected the plasma expander Gelofusin in order to decrease dosage to the kidney, and no renal toxicity was observed. In a comparison study, the ^{177}Lu-DTPA-trastuzumab treatment delivered a 6-fold higher tumor dose, yet the dose to normal organs such as spleen, bone, and blood were much higher (80, 26, and 4180-fold), supporting the use of the smaller 2Rs15d sdAb.

Another recent study evaluated ^{131}I-SGMIB-2Rs15d, which is residualizing, as a theranostic in two HER2-positive cancer models[60]. ^{131}I-SGMIB-2Rs15d successfully detected the tumors by SPECT, and a single dose extended survival with no toxicity and a minimal dose to the kidneys due to its rapid clearance. In the BT474/M1 xenograft model, ^{131}I-SGMIB-2Rs15d extended median survival (140 days) compared to control sdAb (94 days), and in the SKOV-3 metastatic model, median survival was extended 20 days longer than control, or 50 days longer in combination with trastuzumab. Additionally, there was no significant difference in tumor or normal tissue uptake between animals treated with ^{131}I-SGMIB-2Rs15d alone or animals pretreated with trastuzumab, pertuzumab, or both, supporting the potential of using ^{131}I-2Rs15d in patients receiving HER2-targeted therapy.

Diabody—The TAG72-targeting diabody (AVP04-07) in mice bearing LS174T colon cancer carcinoma xenografts was evaluated for RIT[112]. A click chemistry pretargeting strategy was used in order to reduce renal uptake and allow for increased radiation dose to the tumor. Compared to the PEGylation strategy for this diabody, AVP04-07 functionalized with an average of 4.7 TCO groups and one equivalent of ^{177}Lu-TCO yielded the best tumor-targeting results with low renal uptake, tumor-to-kidney ratio of 5.7, and 4-fold improved tumor-to-blood ratio compared to PEGylation strategy.

Minibody—L19-SIP, composed of the recombinant L19 scFv to the C_H4 domain of human IgE, was engineered to target extra domain B of fibronectin[76]. ^{131}I-L19-SIP demonstrated superior therapeutic efficacy compared with dimeric scFv or IgG in teratocarcinoma tumor-bearing mice. For imaging, ^{124}I-L19-SIP was developed as an immunoPET tracer to inform ^{131}I-L19-SIP RIT dosimetry and patient selection in clinical trials, and both ^{124}I and ^{131}I-L19-SIP were further developed in clinical studies[113,114].

In the clinic, ^{124}I-L19-SIP (radretumab) was used to predict dosage delivered to tumors in patients with brain metastases[114]. ^{131}I-L19-SIP was tested as RIT in combination with external beam radiation in patients with multiple brain metastases (NCT01125085), and preliminary results showed reduction in ^{18}F-FDG uptake in 3 of 4 patients[77]. Radretumab was also tested in patients with relapsed hematological cancers, where a diagnostic dose was first used to determine eligibility if tumor uptake was sufficient[78] (Figure 5a). Three of ten patients who received radretumab showed complete response, and the authors suggest patients with advanced lymphomas could benefit from concurrent chemotherapy.

Another humanized SIP, F16, targets tenascin-C expressed at high levels in tumor extracellular matrix. F16-SIP was labeled with ^{131}I and used for RIT in patients with recurrent Hodgkin's lymphoma[79]. ^{18}F-FDG PET and diagnostic ^{131}I-F16-SIP SPECT was used to determine patient eligibility, and after 4–6 weeks several patients had disease stabilization, one patient showed partial response, and one showed complete response (Figure 5b). However, responses were short-lived, and dose fractionation or combination therapy were suggested for future studies.

Bispecific antibodies for pretargeting—One study assessed several bispecific formats engineered via fusion of anti-DOTA scFv to intact anti-CEA M5A mAb at the C-terminal, N-terminal, light chain (LC), or as a dual variable domain immunoglobulin for tumor targeting and pharmacokinetics for pre-targeted RIT in a LS-174T s.c. colon carcinoma model[115]. LC-BsAb and ^{177}Lu-DOTA accumulated specifically in the tumor (6% ID/g) with low normal tissue activity, supporting the use of pretargeting for RIT compared to non-pre-targeted approach, in order to reduce radioactive exposure to sensitive tissues such as bone marrow.

The Tri-Fab TF2 is composed of anti-CEA × anti-HSG which allows for pretargeting of radiolabeled hapten-peptide, IMP-288. TF2 was used for pretargeted radioimmunotherapy (PRIT) in mice bearing CEA-positive colorectal cancer xenografts, where alpha-emitting hapten ^{213}Bi-IMP288 was shown to be at least as effective as beta-emitting hapten ^{177}Lu-IMP288[86]. Tri-Fab pretargeting was extended to the target trophoblast cell surface antigen 2 (TROP2), a transmembrane protein overexpressed in numerous cancers. TF12 is composed of two anti-TROP2 Fabs, along with one anti-HSG Fab that allows for the substitution of a radiolabeled hapten-peptide, IMP-288. In mice bearing s.c. prostate cancer xenografts, TF12 was used with ^{68}Ga-IMP288 for same-day pretargeted immunoPET, and TF12 and ^{177}Lu-IMP288 resulted in successful radioimmunotherapy that extended survival (Figure 5c)[88]. The therapy had decreased toxicity in comparison with ^{177}Lu-anti-TROP2 IgG RIT as measured by decreased platelets and leukocytes.

In a first-in-human Phase I study, anti-CEA × anti-HSG TF2 was evaluated in patients with colorectal cancer, with ^{111}In-IMP288 used in the imaging cycle and ^{177}Lu-IMP288 in the following therapy cycle[87]. In all patients, clear targeting of ^{111}In-IMP288 and TF2 to known CEA-positive lesions was observed by scintigraphic imaging, and patients were allowed to proceed to ^{177}Lu-IMP288 therapy. Optimal targeting was achieved using a lowered IMP288 dose and shortening the interval between administering TF2 and radiolabeled-IMP288 to 1 day. The authors suggest future studies could assess using ^{90}Y as the radiolabel, which may be better for advanced metastatic disease due to its physical half-life that better matches the residence time of the radiopharmaceuticals in the tumor.

Alternative Scaffolds—RIT studies in HER2-expressing tumor models support the development of the Affibody $Z_{HER2:342}$ to treat trastuzumab-resistant HER2+ tumors. Due to the small size, the $Z_{HER2:342}$ clears rapidly and biodistribution studies with residualizing radionuclides show high renal reabsorption. Therefore, fusion to an albumin-binding domain (ABD) was used to reduce renal toxicity and increase circulation for RIT[96]. ^{177}Lu-ABD-$Z_{HER2:342}$ successfully targeted HER2+ microxenografts as confirmed by gamma-camera

imaging, and the treatment extended survival in mice with high and low HER2+ tumors, although overall mortality was caused by bone marrow toxicity. Another approach to reduce high renal activity was to choose a nonresidualizing radiolabel and optimize mercaptoacetyl-containing chelators[97]. The $Z_{HER2:34}$ Affibody showed the lowest renal uptake with ^{99m}Tc and the chelator mercaptoacetyl-glycl-seryl-glycl (maGSG), and therefore it was radiolabeled with the therapeutic chemical analogue ^{186}Re. Specific uptake of ^{186}Re-maGSG-$Z_{HER2:34}$ in HER2+ xenografts was confirmed by biodistribution analysis, with low uptake in normal organs including kidneys. Lastly, another study employed pretargeting to reduce renal absorption of RIT radionuclides, and the biodistribution of anti-HER2 Affibody Z_{2395}-TCO and residualizing radiometals ^{111}In and ^{177}Lu was analyzed[98]. The preliminary dosimetry showed the tumor absorbed dose exceeded the kidney dose 1.4-fold, which is a low therapeutic index and likely would only lead to palliative effects, and the results support future optimization of this pretargeting strategy for RIT.

CONCLUSIONS

Antibodies and fragments are ideal carriers for radionuclide delivery for oncological applications, and protein engineering allows for optimization of half-life, conjugation strategies, and optimal pairing with radionuclides. Advantages of using fragments include rapid tumor uptake and elimination, which limits exposure to normal tissues and increases tumor-to-background ratios and therapeutic indexes. Additionally, removal of Fc-based immunogenicity may ease translation to the clinic. Targeted radionuclide delivery through antibody-based SPECT and PET imaging agents, as well as RIT agents, has been successfully evaluated in preclinical studies and clinical trials as exemplified in this review.

For imaging applications, radiolabeled antibodies and fragments can assess biomarker expression to aid diagnosis, guide therapy selection, monitor therapy, and ultimately allow for personalized medicine. The expanding number of antibodies and fragments in the literature and approved in the clinic target a wide range of biomarkers expressed on diseases such as breast cancer, prostate cancer, and glioblastoma, as well as tumor-associated immune cells such as B cells, T cells, and macrophages. Fragment-based immunoPET can also be applied to address new biological questions, such as relationships between tumors and immune cells in the tumor microenvironment. Additionally, bispecific antibodies enable pretargeting strategies that can improve imaging contrast, and future imaging studies using multispecific antibodies may enable dual-targeting of two markers overexpressed in disease.

Radioimmunotherapy allows for targeted delivery of radiation to disseminated and solid tumors. Factors to consider for successful RIT include disease setting, antigen expression, physical properties of therapeutic radionuclides, and pharmacokinetics of the radiolabeled antibody or fragment. Although RIT has mostly been successful for hematopoietic cancers, solid or radioresistant tumors may be treated using strategies such as pretargeting, which can result in improved therapeutic index. Additionally, doses can be fractionated and administered over a longer period of time, which has been shown to reduce toxicity especially in the hematopoietic system[116]. Lastly, RIT may be used in combination therapy with other agents such as immunotherapy or antibody-drug conjugates[117].

Finally, a single antibody fragment can be radiolabeled with either paired radioisotopes, or a radionuclide with multiple types of emissions such as beta and gamma particles, and be used for both diagnostic and therapeutic applications. A theranostic strategy can quantitatively assess biomarker expression, inform which patients would benefit from the corresponding RIT, and allow for monitoring the effectiveness of the therapy over time. In conclusion, radiolabeled engineered antibodies and fragments are versatile agents that can be clinically translated as diagnostics and therapeutics.

Acknowledgments

The authors thank Dr. Kirstin Zettlitz for her thoughtful review of the manuscript, and grant support from NIH R01 CA174294 and the UCLA Jonsson Comprehensive Cancer Center (NIH P30 CA016042).

References

1. Knowles SM, Wu AM. Advances in immuno-positron emission tomography: antibodies for molecular imaging in oncology. J Clin Oncol. 2012; 30(31):3884–3892. [PubMed: 22987087]
2. Freise AC, Wu AM. In vivo imaging with antibodies and engineered fragments. Mol Immunol. 2015; 67(2 Pt A):142–152. [PubMed: 25934435]
3. Larson SM, Carrasquillo JA, Cheung NK, Press OW. Radioimmunotherapy of human tumours. Nat Rev Cancer. 2015; 15(6):347–360. [PubMed: 25998714]
4. Strohl WR. Current progress in innovative engineered antibodies. Protein Cell. 2017
5. Kaplon H, Reichert JM. Antibodies to watch in 2018. MAbs. 2018:1–21.
6. Wu AM. Engineered antibodies for molecular imaging of cancer. Methods. 2014; 65(1):139–147. [PubMed: 24091005]
7. Strohl WR. Fusion Proteins for Half-Life Extension of Biologics as a Strategy to Make Biobetters. BioDrugs. 2015; 29(4):215–239. [PubMed: 26177629]
8. Muyldermans S. Nanobodies: natural single-domain antibodies. Annu Rev Biochem. 2013; 82:775–797. [PubMed: 23495938]
9. Wu AM. Drug Delivery in Oncology. Wiley-VCH Verlag GmbH & Co. KGaA; 2011. Antibodies for the Delivery of Radionuclides; 411–439.
10. Kontermann RE, Brinkmann U. Bispecific antibodies. Drug Discov Today. 2015; 20(7):838–847. [PubMed: 25728220]
11. Azhar A, Ahmad E, Zia Q, Rauf MA, Owais M, Ashraf GM. Recent advances in the development of novel protein scaffolds based therapeutics. Int J Biol Macromol. 2017; 102:630–641. [PubMed: 28412342]
12. Owens B. Faster, deeper, smaller-the rise of antibody-like scaffolds. Nat Biotechnol. 2017; 35(7): 602–603. [PubMed: 28700554]
13. Boswell CA, Tesar DB, Mukhyala K, Theil FP, Fielder PJ, Khawli LA. Effects of charge on antibody tissue distribution and pharmacokinetics. Bioconjug Chem. 2010; 21(12):2153–2163. [PubMed: 21053952]
14. Sanchez-Crespo A. Comparison of Gallium-68 and Fluorine-18 imaging characteristics in positron emission tomography. Appl Radiat Isot. 2013; 76:55–62. [PubMed: 23063597]
15. Conti M, Eriksson L. Physics of pure and non-pure positron emitters for PET: a review and a discussion. EJNMMI Phys. 2016; 3(1):8. [PubMed: 27271304]
16. Martins CD, Kramer-Marek G, Oyen WJG. Radioimmunotherapy for delivery of cytotoxic radioisotopes: current status and challenges. Expert Opin Drug Deliv. 2018; 15(2):185–196. [PubMed: 28893110]
17. Yong KJ, Milenic DE, Baidoo KE, Brechbiel MW. Mechanisms of Cell Killing Response from Low Linear Energy Transfer (LET) Radiation Originating from (177)Lu Radioimmunotherapy Targeting Disseminated Intraperitoneal Tumor Xenografts. Int J Mol Sci. 2016; 17(5)

18. Kassis AI. Therapeutic radionuclides: biophysical and radiobiologic principles. Semin Nucl Med. 2008; 38(5):358–366. [PubMed: 18662557]
19. Wright CL, Zhang J, Tweedle MF, Knopp MV, Hall NC. Theranostic Imaging of Yttrium-90. Biomed Res Int. 2015; 2015:481279. [PubMed: 26106608]
20. Zalutsky MR, Pozzi OR. Radioimmunotherapy with alpha-particle emitting radionuclides. Q J Nucl Med Mol Imaging. 2004; 48(4):289–296. [PubMed: 15640792]
21. Muller C, van der Meulen NP, Benesova M, Schibli R. Therapeutic Radiometals Beyond 177Lu and 90Y: Production and Application of Promising alpha-Particle, beta--Particle, and Auger Electron Emitters. J Nucl Med. 2017; 58(Suppl 2):91S–96S. [PubMed: 28864619]
22. McDevitt MR, Ma D, Lai LT, et al. Tumor therapy with targeted atomic nanogenerators. Science. 2001; 294(5546):1537–1540. [PubMed: 11711678]
23. Kratochwil C, Bruchertseifer F, Giesel FL, et al. 225Ac-PSMA-617 for PSMA-Targeted alpha-Radiation Therapy of Metastatic Castration-Resistant Prostate Cancer. J Nucl Med. 2016; 57(12): 1941–1944. [PubMed: 27390158]
24. Piron B, Paillas S, Boudousq V, et al. DNA damage-centered signaling pathways are effectively activated during low dose-rate Auger radioimmunotherapy. Nucl Med Biol. 2014; 41(Suppl):e75–83. [PubMed: 24613681]
25. Behr TM, Behe M, Lohr M, et al. Therapeutic advantages of Auger electron-over beta-emitting radiometals or radioiodine when conjugated to internalizing antibodies. Eur J Nucl Med. 2000; 27(7):753–765. [PubMed: 10952487]
26. Salacinski PR, McLean C, Sykes JE, Clement-Jones VV, Lowry PJ. Iodination of proteins, glycoproteins, and peptides using a solid-phase oxidizing agent, 1,3,4,6-tetrachloro-3 alpha,6 alpha-diphenyl glycoluril (Iodogen). Anal Biochem. 1981; 117(1):136–146. [PubMed: 7316186]
27. Vaidyanathan G, Affleck DJ, Li J, Welsh P, Zalutsky MR. A polar substituent-containing acylation agent for the radioiodination of internalizing monoclonal antibodies: N-succinimidyl 4-guanidinomethyl-3-[131I]iodobenzoate ([131I]SGMIB). Bioconjug Chem. 2001; 12(3):428–438. [PubMed: 11353542]
28. Wadas TJ, Wong EH, Weisman GR, Anderson CJ. Coordinating radiometals of copper, gallium, indium, yttrium, and zirconium for PET and SPECT imaging of disease. Chem Rev. 2010; 110(5): 2858–2902. [PubMed: 20415480]
29. Price EW, Orvig C. Matching chelators to radiometals for radiopharmaceuticals. Chem Soc Rev. 2014; 43(1):260–290. [PubMed: 24173525]
30. Pandey U, Gamre N, Lohar SP, Dash A. A systematic study on the utility of CHX-A″-DTPA-NCS and NOTA-NCS as bifunctional chelators for 177Lu radiopharmaceuticals. Appl Radiat Isot. 2017; 127:1–6. [PubMed: 28478331]
31. Tolmachev V, Xu H, Wallberg H, et al. Evaluation of a maleimido derivative of CHX-A″ DTPA for site-specific labeling of affibody molecules. Bioconjug Chem. 2008; 19(8):1579–1587. [PubMed: 18620447]
32. Deri MA, Zeglis BM, Francesconi LC, Lewis JS. PET imaging with (8)(9)Zr: from radiochemistry to the clinic. Nucl Med Biol. 2013; 40(1):3–14. [PubMed: 22998840]
33. Vosjan MJ, Perk LR, Visser GW, et al. Conjugation and radiolabeling of monoclonal antibodies with zirconium-89 for PET imaging using the bifunctional chelate p-isothiocyanatobenzyl-desferrioxamine. Nat Protoc. 2010; 5(4):739–743. [PubMed: 20360768]
34. Vallabhajosula S. The Chemistry of Therapeutic Radiopharmaceuticals. In: Aktolun C, Goldsmith SJ, editorsNuclear Medicine Therapy: Principles and Clinical Applications. New York, NY: Springer New York; 2013. 339–368.
35. Guimaraes CP, Witte MD, Theile CS, et al. Site-specific C-terminal and internal loop labeling of proteins using sortase-mediated reactions. Nat Protoc. 2013; 8(9):1787–1799. [PubMed: 23989673]
36. Adumeau P, Sharma SK, Brent C, Zeglis BM. Site-Specifically Labeled Immunoconjugates for Molecular Imaging--Part 1: Cysteine Residues and Glycans. Mol Imaging Biol. 2016; 18(1):1–17.
37. Richter S, Wuest F. 18F-Labeled Peptides: The Future Is Bright. Molecules. 2014; 19(12):20536–20556. [PubMed: 25493636]

38. Liu K, Lepin EJ, Wang MW, et al. Microfluidic-based 18F-labeling of biomolecules for immuno-positron emission tomography. Mol Imaging. 2011; 10(3):168–176. 161–167. [PubMed: 21496447]
39. Kramer-Marek G, Kiesewetter DO, Martiniova L, Jagoda E, Lee SB, Capala J. [18F]FBEM-Z(HER2:342)-Affibody molecule-a new molecular tracer for in vivo monitoring of HER2 expression by positron emission tomography. Eur J Nucl Med Mol Imaging. 2008; 35(5):1008–1018. [PubMed: 18157531]
40. McBride WJ, Sharkey RM, Karacay H, et al. A novel method of 18F radiolabeling for PET. J Nucl Med. 2009; 50(6):991–998. [PubMed: 19443594]
41. Laverman P, McBride WJ, Sharkey RM, Goldenberg DM, Boerman OC. Al(18) F labeling of peptides and proteins. J Labelled Comp Radiopharm. 2014; 57(4):219–223. [PubMed: 24408125]
42. Pretze M, Pietzsch D, Mamat C. Recent trends in bioorthogonal click-radiolabeling reactions using fluorine-18. Molecules. 2013; 18(7):8618–8665. [PubMed: 23881051]
43. Meyer JP, Houghton JL, Kozlowski P, et al. (18)F-Based Pretargeted PET Imaging Based on Bioorthogonal Diels-Alder Click Chemistry. Bioconjug Chem. 2016; 27(2):298–301. [PubMed: 26479967]
44. Zeglis BM, Sevak KK, Reiner T, et al. A pretargeted PET imaging strategy based on bioorthogonal Diels-Alder click chemistry. J Nucl Med. 2013; 54(8):1389–1396. [PubMed: 23708196]
45. Zeglis BM, Brand C, Abdel-Atti D, et al. Optimization of a Pretargeted Strategy for the PET Imaging of Colorectal Carcinoma via the Modulation of Radioligand Pharmacokinetics. Mol Pharm. 2015; 12(10):3575–3587. [PubMed: 26287993]
46. Luo H, Hernandez R, Hong H, et al. Noninvasive brain cancer imaging with a bispecific antibody fragment, generated via click chemistry. Proc Natl Acad Sci U S A. 2015; 112(41):12806–12811. [PubMed: 26417085]
47. Houghton JL, Membreno R, Abdel-Atti D, et al. Establishment of the In Vivo Efficacy of Pretargeted Radioimmunotherapy Utilizing Inverse Electron Demand Diels-Alder Click Chemistry. Mol Cancer Ther. 2017; 16(1):124–133. [PubMed: 28062708]
48. Reichert JM. Antibodies to watch in 2017. MAbs. 2017; 9(2):167–181. [PubMed: 27960628]
49. Mestel R. Cancer: Imaging with antibodies. Nature. 2017; 543(7647):743–746. [PubMed: 28358075]
50. Ulaner GA, Hyman DM, Ross DS, et al. Detection of HER2-Positive Metastases in Patients with HER2-Negative Primary Breast Cancer Using 89Zr-Trastuzumab PET/CT. J Nucl Med. 2016; 57(10):1523–1528. [PubMed: 27151988]
51. Ulaner GA, Lyashchenko SK, Riedl C, et al. First-in-human HER2-targeted imaging using (89)Zr-pertuzumab PET/CT: Dosimetry and clinical application in patients with breast cancer. J Nucl Med. 2017
52. Holliger P, Hudson PJ. Engineered antibody fragments and the rise of single domains. Nat Biotechnol. 2005; 23(9):1126–1136. [PubMed: 16151406]
53. Chatalic KL, Veldhoven-Zweistra J, Bolkestein M, et al. A Novel (1)(1)(1)In-Labeled Anti-Prostate-Specific Membrane Antigen Nanobody for Targeted SPECT/CT Imaging of Prostate Cancer. J Nucl Med. 2015; 56(7):1094–1099. [PubMed: 25977460]
54. Vaneycken I, Govaert J, Vincke C, et al. In vitro analysis and in vivo tumor targeting of a humanized, grafted nanobody in mice using pinhole SPECT/micro-CT. J Nucl Med. 2010; 51(7):1099–1106. [PubMed: 20554727]
55. Gainkam LO, Huang L, Caveliers V, et al. Comparison of the biodistribution and tumor targeting of two 99mTc-labeled anti-EGFR nanobodies in mice, using pinhole SPECT/micro-CT. J Nucl Med. 2008; 49(5):788–795. [PubMed: 18413403]
56. Vaidyanathan G, McDougald D, Choi J, et al. Preclinical Evaluation of 18F-Labeled Anti-HER2 Nanobody Conjugates for Imaging HER2 Receptor Expression by Immuno-PET. J Nucl Med. 2016; 57(6):967–973. [PubMed: 26912425]
57. Zhou Z, Vaidyanathan G, McDougald D, et al. Fluorine-18 Labeling of the HER2-Targeting Single-Domain Antibody 2Rs15d Using a Residualizing Label and Preclinical Evaluation. Mol Imaging Biol. 2017

58. D'Huyvetter M, Vincke C, Xavier C, et al. Targeted radionuclide therapy with A 177Lu-labeled anti-HER2 nanobody. Theranostics. 2014; 4(7):708–720. [PubMed: 24883121]
59. Keyaerts M, Xavier C, Heemskerk J, et al. Phase I Study of 68Ga-HER2-Nanobody for PET/CT Assessment of HER2 Expression in Breast Carcinoma. J Nucl Med. 2016; 57(1):27–33. [PubMed: 26449837]
60. D'Huyvetter M, De Vos J, Xavier C, et al. 131I-labeled Anti-HER2 Camelid sdAb as a Theranostic Tool in Cancer Treatment. Clin Cancer Res. 2017
61. Rashidian M, Keliher EJ, Bilate AM, et al. Noninvasive imaging of immune responses. Proc Natl Acad Sci U S A. 2015; 112(19):6146–6151. [PubMed: 25902531]
62. Rashidian M, Ingram JR, Dougan M, et al. Predicting the response to CTLA-4 blockade by longitudinal noninvasive monitoring of CD8 T cells. J Exp Med. 2017; 214(8):2243–2255. [PubMed: 28666979]
63. Holliger P, Prospero T, Winter G. "Diabodies": small bivalent and bispecific antibody fragments. Proc Natl Acad Sci U S A. 1993; 90(14):6444–6448. [PubMed: 8341653]
64. Zettlitz KA, Tavare R, Knowles SM, Steward KK, Timmerman JM, Wu AM. ImmunoPET of malignant and normal B cells with 89Zr- and 124I-labeled obinutuzumab antibody fragments reveals differential CD20 internalization in vivo. Clin Cancer Res. 2017
65. Tavare R, McCracken MN, Zettlitz KA, et al. Immuno-PET of Murine T Cell Reconstitution Postadoptive Stem Cell Transplantation Using Anti-CD4 and Anti-CD8 Cys-Diabodies. J Nucl Med. 2015; 56(8):1258–1264. [PubMed: 25952734]
66. Freise AC, Zettlitz KA, Salazar FB, Lu X, Tavare R, Wu AM. ImmunoPET Imaging of Murine CD4+ T Cells Using Anti-CD4 Cys-Diabody: Effects of Protein Dose on T Cell Function and Imaging. Mol Imaging Biol. 2017; 19(4):599–609. [PubMed: 27966069]
67. Tavare R, Escuin-Ordinas H, Mok S, et al. An Effective Immuno-PET Imaging Method to Monitor CD8-Dependent Responses to Immunotherapy. Cancer Res. 2016; 76(1):73–82. [PubMed: 26573799]
68. Viola-Villegas NT, Sevak KK, Carlin SD, et al. Noninvasive Imaging of PSMA in prostate tumors with (89)Zr-Labeled huJ591 engineered antibody fragments: the faster alternatives. Mol Pharm. 2014; 11(11):3965–3973. [PubMed: 24779727]
69. Sundaresan G, Yazaki PJ, Shively JE, et al. 124I-labeled engineered anti-CEA minibodies and diabodies allow high-contrast, antigen-specific small-animal PET imaging of xenografts in athymic mice. J Nucl Med. 2003; 44(12):1962–1969. [PubMed: 14660722]
70. Yazaki PJ, Wu AM, Tsai SW, et al. Tumor targeting of radiometal labeled anti-CEA recombinant T84.66 diabody and t84.66 minibody: comparison to radioiodinated fragments. Bioconjug Chem. 2001; 12(2):220–228. [PubMed: 11312683]
71. Tavare R, McCracken MN, Zettlitz KA, et al. Engineered antibody fragments for immuno-PET imaging of endogenous CD8+ T cells in vivo. Proc Natl Acad Sci U S A. 2014; 111(3):1108–1113. [PubMed: 24390540]
72. Knowles SM, Tavare R, Zettlitz KA, et al. Applications of immunoPET: using 124I-anti-PSCA A11 minibody for imaging disease progression and response to therapy in mouse xenograft models of prostate cancer. Clin Cancer Res. 2014; 20(24):6367–6378. [PubMed: 25326233]
73. Knowles SM, Zettlitz KA, Tavare R, et al. Quantitative immunoPET of prostate cancer xenografts with 89Zr- and 124I-labeled anti-PSCA A11 minibody. J Nucl Med. 2014; 55(3):452–459. [PubMed: 24504052]
74. Pandit-Taskar N, O'Donoghue JA, Ruan S, et al. First-in-Human Imaging with 89Zr-Df-IAB2M Anti-PSMA Minibody in Patients with Metastatic Prostate Cancer: Pharmacokinetics, Biodistribution, Dosimetry, and Lesion Uptake. J Nucl Med. 2016
75. Hu S, Shively L, Raubitschek A, et al. Minibody: A novel engineered anti-carcinoembryonic antigen antibody fragment (single-chain Fv-CH3) which exhibits rapid, high-level targeting of xenografts. Cancer Res. 1996; 56(13):3055–3061. [PubMed: 8674062]
76. Berndorff D, Borkowski S, Sieger S, et al. Radioimmunotherapy of solid tumors by targeting extra domain B fibronectin: identification of the best-suited radioimmunoconjugate. Clin Cancer Res. 2005; 11(19 Pt 2):7053s–7063s. [PubMed: 16203802]

77. Virotta G, Poli GL, Bettini A, et al. Radioimmunotherapy with 131I-L19SIP (Radretumab) in metastatic solid tumors: Preliminary results. Journal of Nuclear Medicine. 2012; 53(supplement 1):498.

78. Erba PA, Sollini M, Orciuolo E, et al. Radioimmunotherapy with Radretumab in Patients with Relapsed Hematologic Malignancies. Journal of Nuclear Medicine. 2012

79. Aloj L, D'Ambrosio L, Aurilio M, et al. Radioimmunotherapy with Tenarad, a 131I-labelled antibody fragment targeting the extra-domain A1 of tenascin-C, in patients with refractory Hodgkin's lymphoma. Eur J Nucl Med Mol Imaging. 2014; 41(5):867–877. [PubMed: 24435772]

80. Brinkmann U, Kontermann RE. The making of bispecific antibodies. MAbs. 2017; 9(2):182–212. [PubMed: 28071970]

81. Trivedi A, Stienen S, Zhu M, et al. Clinical Pharmacology and Translational Aspects of Bispecific Antibodies. Clin Transl Sci. 2017; 10(3):147–162. [PubMed: 28297195]

82. Hoffman LM, Gore L. Blinatumomab, a Bi-Specific Anti-CD19/CD3 BiTE((R)) Antibody for the Treatment of Acute Lymphoblastic Leukemia: Perspectives and Current Pediatric Applications. Front Oncol. 2014; 4:63. [PubMed: 24744989]

83. Liu L, Lam CK, Long V, et al. MGD011, A CD19 × CD3 Dual-Affinity Retargeting Bi-specific Molecule Incorporating Extended Circulating Half-life for the Treatment of B-Cell Malignancies. Clin Cancer Res. 2017; 23(6):1506–1518. [PubMed: 27663593]

84. Mullard A. Bispecific antibody pipeline moves beyond oncology. Nat Rev Drug Discov. 2017; 16(11):810.

85. Altai M, Membreno R, Cook B, Tolmachev V, Zeglis B. Pretargeted Imaging and Therapy. J Nucl Med. 2017

86. Heskamp S, Hernandez R, Molkenboer-Kuenen JDM, et al. alpha- Versus beta-Emitting Radionuclides for Pretargeted Radioimmunotherapy of Carcinoembryonic Antigen-Expressing Human Colon Cancer Xenografts. J Nucl Med. 2017; 58(6):926–933. [PubMed: 28232604]

87. Schoffelen R, Boerman OC, Goldenberg DM, et al. Development of an imaging-guided CEA-pretargeted radionuclide treatment of advanced colorectal cancer: first clinical results. Br J Cancer. 2013; 109(4):934–942. [PubMed: 23860529]

88. van Rij CM, Lutje S, Frielink C, et al. Pretargeted immuno-PET and radioimmunotherapy of prostate cancer with an anti-TROP-2 × anti-HSG bispecific antibody. Eur J Nucl Med Mol Imaging. 2013; 40(9):1377–1383. [PubMed: 23674207]

89. Lofblom J, Feldwisch J, Tolmachev V, Carlsson J, Stahl S, Frejd FY. Affibody molecules: engineered proteins for therapeutic, diagnostic and biotechnological applications. FEBS Lett. 2010; 584(12):2670–2680. [PubMed: 20388508]

90. Frejd FY, Kim KT. Affibody molecules as engineered protein drugs. Exp Mol Med. 2017; 49(3):e306. [PubMed: 28336959]

91. Orlova A, Magnusson M, Eriksson TL, et al. Tumor imaging using a picomolar affinity HER2 binding affibody molecule. Cancer Res. 2006; 66(8):4339–4348. [PubMed: 16618759]

92. Orlova A, Wallberg H, Stone-Elander S, Tolmachev V. On the selection of a tracer for PET imaging of HER2-expressing tumors: direct comparison of a 124I-labeled affibody molecule and trastuzumab in a murine xenograft model. J Nucl Med. 2009; 50(3):417–425. [PubMed: 19223403]

93. Baum RP, Prasad V, Muller D, et al. Molecular imaging of HER2-expressing malignant tumors in breast cancer patients using synthetic 111In- or 68Ga-labeled affibody molecules. J Nucl Med. 2010; 51(6):892–897. [PubMed: 20484419]

94. Sorensen J, Sandberg D, Sandstrom M, et al. First-in-human molecular imaging of HER2 expression in breast cancer metastases using the 111In-ABY-025 affibody molecule. J Nucl Med. 2014; 55(5):730–735. [PubMed: 24665085]

95. Sorensen J, Velikyan I, Sandberg D, et al. Measuring HER2-Receptor Expression In Metastatic Breast Cancer Using [68Ga]ABY-025 Affibody PET/CT. Theranostics. 2016; 6(2):262–271. [PubMed: 26877784]

96. Tolmachev V, Orlova A, Pehrson R, et al. Radionuclide therapy of HER2-positive microxenografts using a 177Lu-labeled HER2-specific Affibody molecule. Cancer Res. 2007; 67(6):2773–2782. [PubMed: 17363599]

97. Orlova A, Tran TA, Ekblad T, Karlstrom AE, Tolmachev V. (186)Re-maSGS-Z (HER2:342), a potential Affibody conjugate for systemic therapy of HER2-expressing tumours. Eur J Nucl Med Mol Imaging. 2010; 37(2):260–269. [PubMed: 19771426]

98. Altai M, Perols A, Tsourma M, et al. Feasibility of Affibody-Based Bioorthogonal Chemistry-Mediated Radionuclide Pretargeting. J Nucl Med. 2016; 57(3):431–436. [PubMed: 26659353]

99. Movahedi K, Schoonooghe S, Laoui D, et al. Nanobody-based targeting of the macrophage mannose receptor for effective in vivo imaging of tumor-associated macrophages. Cancer Res. 2012; 72(16):4165–4177. [PubMed: 22719068]

100. Blykers A, Schoonooghe S, Xavier C, et al. PET Imaging of Macrophage Mannose Receptor-Expressing Macrophages in Tumor Stroma Using 18F-Radiolabeled Camelid Single-Domain Antibody Fragments. J Nucl Med. 2015; 56(8):1265–1271. [PubMed: 26069306]

101. Cai W, Olafsen T, Zhang X, et al. PET imaging of colorectal cancer in xenograft-bearing mice by use of an 18F-labeled T84.66 anti-carcinoembryonic antigen diabody. J Nucl Med. 2007; 48(2): 304–310. [PubMed: 17268029]

102. Lutje S, Franssen GM, Sharkey RM, et al. Anti-CEA antibody fragments labeled with [(18)F]AlF for PET imaging of CEA-expressing tumors. Bioconjug Chem. 2014; 25(2):335–341. [PubMed: 24382090]

103. Eder M, Knackmuss S, Le Gall F, et al. 68Ga-labelled recombinant antibody variants for immuno-PET imaging of solid tumours. Eur J Nucl Med Mol Imaging. 2010; 37(7):1397–1407. [PubMed: 20157706]

104. Kampmeier F, Williams JD, Maher J, Mullen GE, Blower PJ. Design and preclinical evaluation of a 99mTc-labelled diabody of mAb J591 for SPECT imaging of prostate-specific membrane antigen (PSMA). EJNMMI Res. 2014; 4(1):13. [PubMed: 24602403]

105. Wong P, Li L, Chea J, et al. Synthesis, Positron Emission Tomography Imaging, and Therapy of Diabody Targeted Drug Lipid Nanoparticles in a Prostate Cancer Murine Model. Cancer Biother Radiopharm. 2017; 32(7):247–257. [PubMed: 28910151]

106. Wong JY, Chu DZ, Williams LE, et al. Pilot trial evaluating an 123I-labeled 80-kilodalton engineered anticarcinoembryonic antigen antibody fragment (cT84.66 minibody) in patients with colorectal cancer. Clin Cancer Res. 2004; 10(15):5014–5021. [PubMed: 15297402]

107. Luo H, England CG, Goel S, et al. ImmunoPET and Near-Infrared Fluorescence Imaging of Pancreatic Cancer with a Dual-Labeled Bispecific Antibody Fragment. Molecular Pharmaceutics. 2017

108. Jiang L, Kimura RH, Miao Z, et al. Evaluation of a (64)Cu-labeled cystine-knot peptide based on agouti-related protein for PET of tumors expressing alphavbeta3 integrin. J Nucl Med. 2010; 51(2):251–258. [PubMed: 20124048]

109. Stahl S, Graslund T, Eriksson Karlstrom A, Frejd FY, Nygren PA, Lofblom J. Affibody Molecules in Biotechnological and Medical Applications. Trends Biotechnol. 2017; 35(8):691–712. [PubMed: 28514998]

110. Rosestedt M, Andersson KG, Mitran B, et al. Affibody-mediated PET imaging of HER3 expression in malignant tumours. Sci Rep. 2015; 5:15226. [PubMed: 26477646]

111. Bodet-Milin C, Faivre-Chauvet A, Carlier T, et al. Immuno-PET Using Anticarcinoembryonic Antigen Bispecific Antibody and 68Ga-Labeled Peptide in Metastatic Medullary Thyroid Carcinoma: Clinical Optimization of the Pretargeting Parameters in a First-in-Human Trial. J Nucl Med. 2016; 57(10):1505–1511. [PubMed: 27230928]

112. van Duijnhoven SM, Rossin R, van den Bosch SM, Wheatcroft MP, Hudson PJ, Robillard MS. Diabody Pretargeting with Click Chemistry In Vivo. J Nucl Med. 2015; 56(9):1422–1428. [PubMed: 26159589]

113. Tijink BM, Perk LR, Budde M, et al. (124)I-L19-SIP for immuno-PET imaging of tumour vasculature and guidance of (131)I-L19-SIP radioimmunotherapy. Eur J Nucl Med Mol Imaging. 2009; 36(8):1235–1244. [PubMed: 19259661]

114. Poli GL, Bianchi C, Virotta G, et al. Radretumab radioimmunotherapy in patients with brain metastasis: a 124I-L19SIP dosimetric PET study. Cancer Immunol Res. 2013; 1(2):134–143. [PubMed: 24777501]

115. Yazaki PJ, Lee B, Channappa D, et al. A series of anti-CEA/anti-DOTA bispecific antibody formats evaluated for pre-targeting: comparison of tumor uptake and blood clearance. Protein Eng Des Sel. 2013; 26(3):187–193. [PubMed: 23175797]

116. DeNardo GL, Schlom J, Buchsbaum DJ, et al. Rationales, evidence, and design considerations for fractionated radioimmunotherapy. Cancer. 2002; 94(4 Suppl):1332–1348. [PubMed: 11877764]

117. Sharkey RM, Karacay H, Govindan SV, Goldenberg DM. Combination radioimmunotherapy and chemoimmunotherapy involving different or the same targets improves therapy of human pancreatic carcinoma xenograft models. Mol Cancer Ther. 2011; 10(6):1072–1081. [PubMed: 21467164]

118. Srivastava SC, Mausner LF. Therapeutic Radionuclides: Production, Physical Characteristics, and Applications. In: Baum RP, editorTherapeutic Nuclear Medicine. Berlin, Heidelberg: Springer Berlin Heidelberg; 2014. 11–50.

119. The NUDAT/PCNUDAT Program for Nuclear Data. 1996. http://www.nndc.bnl.gov/

120. Sgouros G, Roeske JC, McDevitt MR, et al. MIRD Pamphlet No. 22 (abridged): radiobiology and dosimetry of alpha-particle emitters for targeted radionuclide therapy. J Nucl Med. 2010; 51(2): 311–328. [PubMed: 20080889]

121. International Atomic Energy Agency DoP, Chemical S, Division of Human Health V. Report of a Technical Meeting on “Alpha emitting radionuclides and radiopharmaceuticals for therapy”. 2013:75.

122. Gray T. IsotopeData. http://www.periodictable.com/

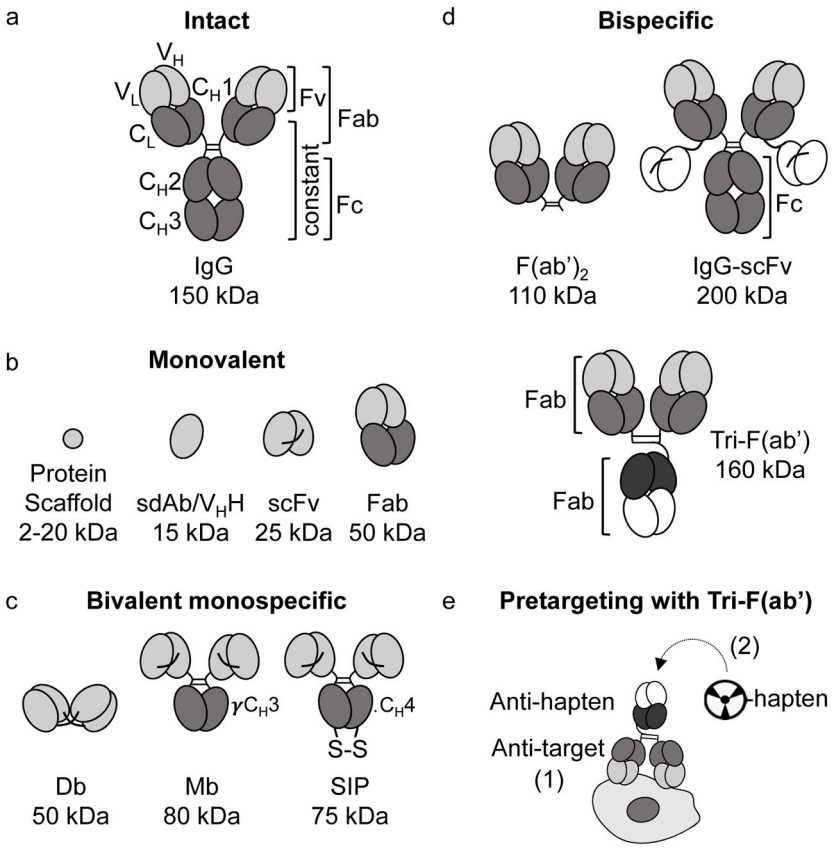

Figure 1. Intact antibody and engineered antibody fragments

Compared to A, intact IgG antibody, engineered antibody fragments range in size, specificity, avidity, and therefore pharmacokinetic properties. Several fragments and scaffolds for radionuclide delivery have been explored in preclinical and clinical studies, including B, monovalent antibody fragments, C, bivalent monospecific fragments, and D, bispecific fragments. E, Schematic of pretargeting strategy using bispecific tri-F(ab′): (1) Tri-F(ab′) binds to target, and subsequently (2) radiolabeled hapten is administered, which rapidly localizes to the Tri-F(ab′) and binds the anti-hapten Fab. Abbreviations: CH= constant heavy, CL= constant light, Db = diabody, Fv= fragment variable, Fab= fragment-antigen binding, Fc= fragment crystallizable, IgG = immunoglobulin G, Mb = minibody, scFv = single chain fragment variable, sdAb= single domain antibody, SIP = small immunoprotein, Tri-F(ab′) = trivalent Fab, VH= variable heavy, VHH= variable heavy, VL= variable light.

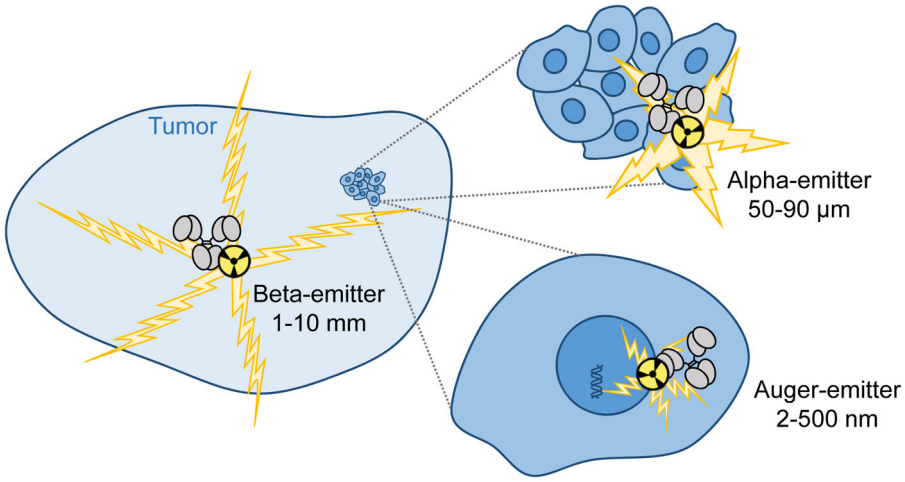

Figure 2. Schematic representation of therapeutic radionuclides

Beta-emitters have a low linear energy transfer (LET) of 0.2 keV/mm and a path length of 1 to 10 mm, and beta emission may reach throughout the tumor and surrounding healthy tissue. Alpha-emitters have a high LET (80–100 keV/μm) and a path length of 50–90 μm, which corresponds to a few cell diameters. Auger-emitters have low energy but high LET (4–26 keV/μm) and a short path length of 2 to 500 nm. Intracellular deposit near the nucleus is necessary for therapeutic effect.

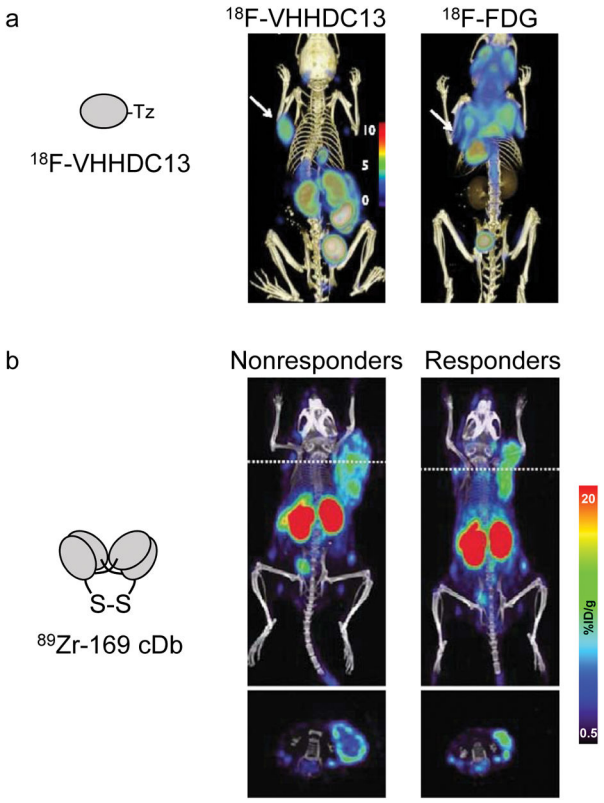

Figure 3. Antibody fragment-based immunoPET imaging of immune cells

A, VHHDC13 (anti-mouse CD11b) is a single domain antibody with an LPETG sortase recognition moiety that can be undergo a transpeptidase reaction to produce VHHDC13-tetrazine. This allows for site specific radiolabeling using ^{18}F-TCO. ^{18}F-VHHDC13 immunoPET shows high contrast targeting of CD11b-positive cells in mice bearing B16 melanoma s.c. tumors. In comparison, ^{18}F-FDG PET shows low contrast between the tumor and background tissues.[61] B, Mice bearing CTD26 xenografts received anti-PD-L1 checkpoint blockade therapy and divided into two groups, responders and nonresponders. ^{89}Zr-anti-CD8 169 cys-diabody immunoPET shows uptake in the rim of the tumor of anti-PD-L1 nonresponders, and intratumoral uptake in responders.[67]

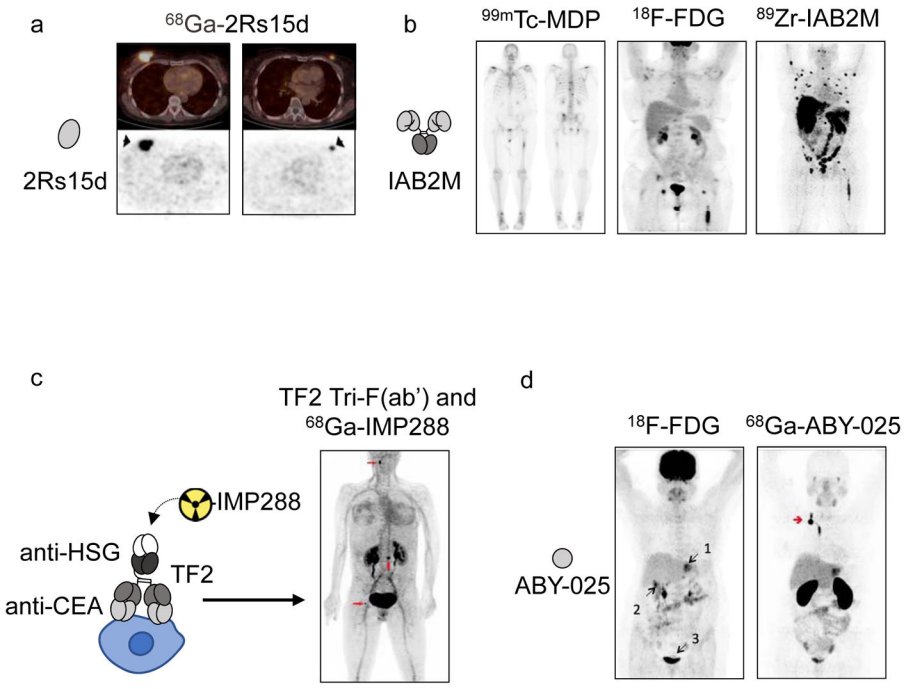

Figure 4. Clinical evaluation of antibody fragments for immunoPET

A, First in human Phase I study of ^{68}Ga-2Rs15d, an anti-HER2 Nanobody, was conducted in patients with breast cancer. Uptake is detected in HER2 primary lesions as shown by PET/CT (top) and PET (bottom) in two patients.[59] B, First-in-human Phase I study of ^{89}Zr-anti-PSMA-IAB2M minibody was conducted in patients with metastatic prostate cancer. ^{99m}Tc-methylene diphosphonate (MDP) bone scan detected lesions in the vertebrae and ribs, ^{18}F-fluorodeoxyglucose (FDG) imaging detected lesions in femur and vertebrae, and ^{89}Zr-IAB2M immunoPET detected soft tissue and bone lesions not identified by the previous two methods.[74] C, Clinical evaluation of bispecific trivalent antibody (BsMAb) TF2 and ^{68}Ga-IMP288 in patients with medullary thyroid carcinoma (MTC). TF2 is composed of two anti-carcinoembryonic antigen (CEA) Fab fragments and one anti-histamine-succinyl-glycine (HSG) Fab fragment, and was administered as the pretargeting agent. IMP288 is a bivalent HSG hapten, and the preferred ^{68}Ga-IMP288 parameter used was a BsMab-to-peptide molar ratio of 20 and 30 h pretargeting delay. ImmunoPET images were acquired 1- and 2- hours post-IMP288-injection. Arrows point to uptake in cervical node, lumbar node and femoral bone foci.[111] D, Clinical evaluation of ^{68}Ga-anti-HER2 ABY-025 Affibody in patients with metastatic breast cancer. The patient shown had HER2-negative primary tumor, and ^{18}F-FDG PET showed uptake in 3 lesions located in the liver, lymph node, and cervix. ^{68}Ga-ABY-025 immunoPET detected the liver lesion, which was confirmed to be HER2-positive by immunohistochemistry (IHC), while the other two lesions were confirmed to be true negative. Red arrow indicates location of portacath used for injection.[95]

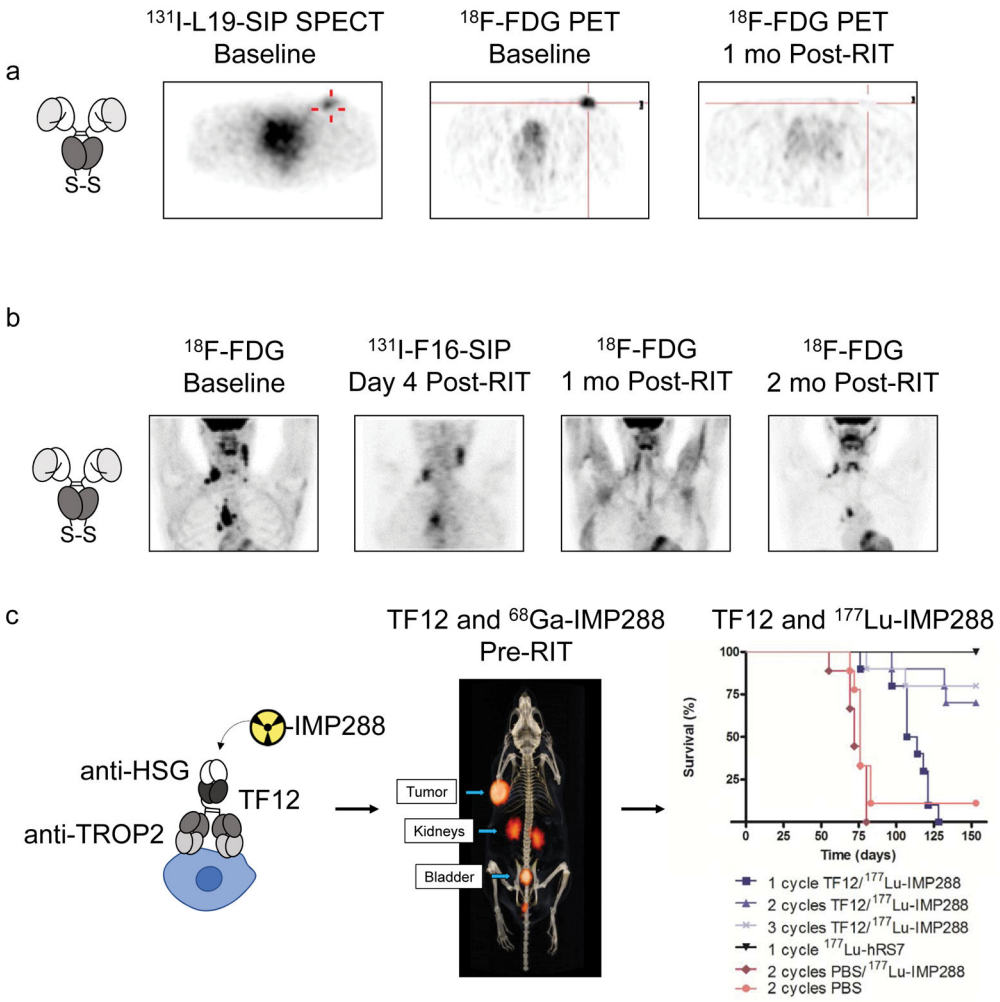

Figure 5. Clinical and preclinical applications of antibody-based radioimmunotherapy

A, ^{131}I-L19-SIP was administered to patients for RIT, this example patient with diffuse large B-cell lymphoma showed a complete response. After a single administration of ^{131}I-L19-SIP, baseline transaxial SPECT and ^{18}F-FDG PET show high uptake in the left inguinal lymphoma, and 1 month post-RIT no uptake is detected by ^{18}F-FDG PET.[78] B, In a patient with refractory Hodgkin's lymphoma, baseline ^{18}F-FDG PET shows uptake in lesions in the neck and mediastinum corresponding to uptake seen at day 4 post-injection of ^{131}I-F16-SIP SPECT. At 1- and 2-month post-injection, ^{18}F-FDG PET images show reduction in uptake.[79] C, Pretargeting strategy with anti-TROP2 × anti-HSG bispecific TF12 and radiolabeled IMP288 HSG hapten. TF12 and ^{68}Ga-IMP288 PET/CT of a BALB/c nude mice bearing s.c. PC3 tumors shows uptake in the tumor, kidneys, and bladder at 1-hour post-injection. Mice were treated with TF12 and ^{177}Lu-IMP288, and survival was extended compared to ^{177}Lu-control vehicle and ^{177}Lu-IMP288 without pretargeting.[88]

Table 1

Radionuclides for imaging

Radionuclide	$t_{1/2}$, (h)	Energy (intensity)	Additional considerations	Reference
Single-photon emitters		**Principal γ energy (keV) (intensity %)**		9, 118,119
^{99m}Tc	6.0	140 keV (98.6%)		
^{111}In	67.2	245 keV (94%) 171 keV (91%)	Auger: 2.8 keV (11%)	
^{123}I	13.1	159 keV (83%)	Auger: 3.2 keV (95%)	
^{131}I	193	364 keV (81%)	β^-: 191 keV (90%)	
^{177}Lu	161	208 keV (11%)	β^-: (149 keV (80%)	
^{67}Cu	62	184 keV (49%)	β^-: (1221 keV (57%)	
^{186}Re	90	137 keV (10%)	β^-: (359 keV (71%)	
^{188}Re	17	155 keV (15%)	β^-: (795 keV (70%)	
Positron emitters		**Principal β^+ energy (keV) (intensity %)**		15,119
^{68}Ga	1.1	836 keV (88%)		
^{18}F	1.8	250 keV (97%)		
^{64}Cu	12.7	278 keV (18%)	β^- (190 keV, 39%)	
^{89}Zr	78.5	396 keV (23%)		
^{124}I	100.3	687 keV (12%) 974 keV (11%)		

J Labelled Comp Radiopharm. Author manuscript; available in PMC 2019 July 01.

Table 2

Radionuclides for therapy

Radionuclide	$t_{1/2}$	Maximum particle range	Energy (intensity)	Additional Considerations	Reference
Auger emitters			**Principal Auger L, K energy (keV) (intensity %)**		9, 21,118,119
^{67}Ga	3.3 d	10 nm	1.0 keV (168%) 7.5 keV (61%)	Pairs with ^{68}Ga	
^{125}I	60 d	10 nm	3.2 keV (157%) 23 keV (20%)		
^{111}In	2.8 d	10 nm	2.8 keV (11%) 20 keV (1.6%)	Imageable γ	
^{161}Tb	4.1 h	0.5–30 μm	5.2 keV (88%) 37 keV (1.5%)	Pairs with ^{152}Tb PET or ^{155}Tb SPECT β⁻: 157 keV (65%)	
Alpha emitters			**Principal α energy (keV) (intensity %)**		118, 119, 118,120–122
^{212}Bi	1.0 h	87 μm	6340 keV (35%) 6300 keV (26%)	1 α-emitting daughter 1 β⁻-emitting daughter Imageable γ	
^{213}Bi	46 min	80 μm	8375 keV (98%) 5870 keV (2%)	2 α-emitting daughters 2 β⁻-emitting daughters Imageable γ	
^{223}Ra	11.4 d	46 μm	5720 keV (52%) 5600 keV (25%)	3 α-emitting daughters 2 β⁻-emitting daughters	
^{221}At	7.2 h	55–70 μm	5870 keV (42%)	4 α-emitting daughters 3 β⁻-emitting daughters Auger: 8.52 keV, 61.2 keV	
^{225}Ac	10.0 d	85 μm	5830 keV (50%) 5790 keV (18%)	4 α-emitting daughters 3 β⁻-emitting daughters (1 daughter emits both α and β⁻) Imageable γ	
^{149}Tb	4.1 h	25 μm	3970 keV (17%)	No α or β⁻-emitting daughters	
Beta emitters			**Principal β⁻ energy (keV) (intensity %)**		9, 21,119
^{177}Lu	6.7 d	1.5 mm	149 keV (80%)	Imageable γ	
^{131}I	8.0 d	2 mm	191 keV (90%)	Imageable γ pairs with ^{124}I PET	
^{90}Y	2.7 d	11.0 mm	934 keV (>99%)	Bremsstrahlung: 0–2.280 MeV	
^{67}Cu	2.6 d	1.8 mm	1220 keV (57%) 468 keV (22%) 189 keV (20%)	Imageable γ pairs with ^{64}Cu PET	

Radionuclide	$t_{1/2}$	Maximum particle range	Energy (intensity)	Additional Considerations	Reference
^{47}Sc	3.3 d	0.2 mm	143 keV (68%) 204 keV (32%)	Pairs with ^{44}Sc PET	
^{166}Ho	1.1 d	8.7 mm	651 keV (50%) 694 keV (49%)	Imageable γ	
^{161}Tb	6.9 d	1.8 mm	157 keV (65%) 138 keV (26%)	Pairs with ^{152}Tb PET or ^{155}Tb SPECT Auger: 5.2 keV (88%)	